



# Solvent molecule mobilities in propylene carbonate-based electrolyte solutions coexisting with fumed oxide nanoparticles

Maki, Hideshi  
Takemoto, Marie  
Sogawa, Ren  
Mizuhata, Minoru

---

## (Citation)

Colloids and Surfaces A: Physicochemical and Engineering Aspects, 562:270-279

## (Issue Date)

2019-02-05

## (Resource Type)

journal article

## (Version)

Accepted Manuscript

## (Rights)

© 2018 Elsevier B.V.

This manuscript version is made available under the CC-BY-NC-ND 4.0 license

<http://creativecommons.org/licenses/by-nc-nd/4.0/>

## (URL)

<https://hdl.handle.net/20.500.14094/90007531>



# Solvent molecule mobilities in propylene carbonate-based electrolyte solutions coexisting with fumed oxide nanoparticles

Hideshi Maki<sup>a,b,\*</sup>, Marie Takemoto<sup>b</sup>, Ren Sogawa<sup>b</sup> and Minoru Mizuhata<sup>b</sup>

*<sup>a</sup>Center for Environmental Management, Kobe University, 1-1 Rokkodai-cho, Nada-ku, Kobe 657-8501, Japan*

*<sup>b</sup>Department of Chemical Science and Engineering, Graduate School of Engineering, Kobe University, 1-1 Rokkodai-cho, Nada-ku, Kobe 657-8501, Japan*

## CORRESPONDING AUTHOR FOOTNOTE

E-mail: maki@kobe-u.ac.jp

## Keywords:

Solvation; Interface; Lithium ion battery; NMR relaxation; LIB; Secondary battery

## ABSTRACT

Non-aqueous LiClO<sub>4</sub> solutions kneaded with various fumed oxides (fumed silica, fumed alumina, and fumed titania) were employed as model systems of lithium ion batteries. The properties of the solid phase and Li<sup>+</sup> ions, which affect solvent molecules, were evaluated using <sup>1</sup>H NMR spectroscopy and <sup>1</sup>H NMR relaxation time (*T*<sub>1</sub>, *T*<sub>2</sub>) measurements. The <sup>1</sup>H NMR signals of propylene carbonate (PC) molecules were influenced by the coexisting solid phase in the LiClO<sub>4</sub>-PC solution/fumed oxide nanoparticle dispersion. The mobilities of the PC molecules drastically decreased in the presence of only 1–2 vol% of the solid phase (liquid phase thickness is 15–20 nm or less), regardless of the fumed oxide employed. In the IR spectra of the PC/fumed alumina systems, the vibrations at higher wavenumbers were predominantly observed because of indirect electron-donation

from the solid surface. The  $^1\text{H}$  NMR signal detection ratios depended on the fraction of the liquid phase influenced by the solid phase. In the  $\text{LiClO}_4$ -PC solution/fumed alumina systems, the  $^1\text{H}$  NMR signal detection ratios greatly decreased because of this influence; here, the large positive zeta potential of the solid phase surface of fumed alumina attracted the PC molecules, which had local negative electric fields owing to polarization. Moreover, the  $T_1$  and  $T_2$  results confirmed that the interaction between the solid phase and PC molecules is much smaller than that between the solid phase and water molecules. Additionally, it was seen that the PC solution system was more significantly affected than the aqueous solution system; the network structure of the entire PC solvent is greatly affected by the addition of the  $\text{Li}^+$  ion, and the relaxation time decreased significantly.

## 1. Introduction

In recent years, lithium ion batteries (LIBs) have become indispensable in various electrochemical devices, such as mobile phones and electric vehicles, because of their high energy density and high voltage. However, to further improve the performance of such electrochemical devices, the capacity and charge/discharge rate of LIBs should be increased. In several electrochemical devices, porous solid materials are fabricated for holding the electrolyte solutions [1–3].

Various studies have reported that the physical properties of a liquid in the neighborhood of a solid surface differ from those of the bulk solution [4–8]. Specifically, the physical properties of the solvent molecules within the pores of a porous material with a layered structure are very different from those in the bulk phase as a result of the extremely small pore volume and large specific surface area [9–11]. Electrolyte solutions subject to ion–solvent interactions exhibit different properties in the presence of a solid phase, and an elucidation of liquid phase properties of the solid–liquid interface in non-aqueous electrolyte solution systems is important for improving the performance of energy storage devices such as LIBs [11,12].

Moreover, it is essential to investigate the properties of high-concentration electrolytes for enhancing the performance of LIBs. In recent years, the study of new materials that utilize highly concentrated electrolytes has attracted attention [13–17]. Yamada et al. have reported that highly concentrated electrolytes improved the charge efficiency and breakdown voltage of LIBs [18]. Various measurement techniques such as thermodynamic measurements [5,19,20], spectrophotometric methods (e.g., Infrared and Raman spectrometries [6,19,21–24], neutron scattering method [25], and X-ray scattering measurements [26]), and electrochemical measurement (e.g., electric conductivity measurement [7,19] and electrochemical impedance spectroscopy) has been used so far. Herein, we focus on NMR measurements in particular. The NMR spectra yield information about the structural changes such as hydrogen bond networks [27]. In addition, information regarding the interactions between a solvent molecule and a solid surface can be obtained from the NMR chemical shift [27–29]. NMR has been used to study several important phenomena of chemistry related to the dynamic time-dependent nature of various systems, particularly those at equilibrium and where simple molecular mobilities are involved. The magnetic relaxation behavior of the nuclear spins is related to the molecular dynamics of the system, and hence, it is a useful parameter for an in-depth study of molecular mobilities in a system. The magnetic relaxation time (spin–lattice magnetic relaxation time,  $T_1$ , and spin–spin relaxation time,  $T_2$ ) is closely related to the rotational correlation time of a molecule [30–32]. In the case of a solid–liquid coexisting system, the rotational correlation times of the solvent and ion molecules increase when their mobilities decrease because of the interaction with a solid phase surface, and as a result,  $T_1$  and  $T_2$  decrease. In the case of a dipolar nucleus such as the  $^1\text{H}$  nucleus, the magnetic relaxation is determined solely from the rotational correlation time of the molecule.

In this study, we prepared high-concentration propylene carbonate (PC) solutions of  $\text{LiClO}_4$ , which were kneaded with fumed silica, fumed alumina, or fumed titania, as model systems of LIBs. Then, the influence of the liquid phase fraction, apparent average liquid phase thickness, and  $\text{LiClO}_4$  concentration on the mobility of a PC molecule were investigated by analyzing the magnetic relaxation

time,  $^1\text{H}$  NMR signal detection ratio of PC molecules, and FT–IR spectra. Furthermore, the effect of the zeta potential at the surface of the fumed oxide nanoparticles on the mobility of a PC molecule was discussed.

## 2. Experimental section

### 2.1. Solid-liquid coexisting model system samples

Fumed silica (FS; AEROSIL® 200CF, Evonik Industries AG, Germany ( $200 \pm 25 \text{ m}^2 \text{ g}^{-1}$ )), fumed alumina (FA; AEROXIDE® Alu 130, Evonik Industries AG, Germany ( $130 \pm 20 \text{ m}^2 \text{ g}^{-1}$ )), or fumed titania (FT; AEROXIDE® TiO<sub>2</sub> P 90, Evonik Industries AG, Germany ( $90 \pm 20 \text{ m}^2 \text{ g}^{-1}$ )) powder whose physical properties are shown in Table S1 was used as solid phases, and propylene carbonate (PC) or 1–3 mol L<sup>−1</sup> LiClO<sub>4</sub> PC solution was used as liquid phase. The surfaces of FS, FA, and FT particles does not have porous structure and are relatively smooth. Paramagnetic impurity ions were not detected from the washing water by a coupled plasma-optical emission spectrometry (ICP-OES). The solid-liquid coexisting model samples were prepared in Ar glovebox by adequate kneading in inner NMR tubes of a coaxial NMR tube system which is shown in Scheme S1. In addition, the solid-liquid coexisting model sample whose solid phase and liquid phase are FS and pure water was also prepared. The coaxial NMR tube system consists of a borosilicate inner (516-I-5, Wilmad-LabGlass, USA) and outer (516-O-5, Wilmad-LabGlass, USA) NMR tubes, and the sample solution and a deuterated solvent for a field-frequency locking (i.e., D<sub>2</sub>O in this work) were put into the inner and outer NMR tube, respectively. Consequently, D<sub>2</sub>O was not contained in the sample solution at all. The FS, FA, or FT powder was homogeneously dispersed in the liquid phases, respectively. The liquid phase fraction,  $\phi_L$ , of the model samples which was determined by a gravimetry was varied in 90–100 vol%. The  $\phi$  values are defined as following equation;

$$\text{Liquid phase fraction } (\phi_L) = V_L / (V_L + V_S) \quad (1)$$

where  $V_L$  and  $V_S$  are the volume of liquid and solid phases, respectively. In this work, the  $V_L$  and  $V_S$  values are determined from the following equations, respectively;

$$V_L = W_L / \rho_L \quad (2)$$

$$V_S = W_S / \rho_S \quad (3)$$

where  $W_L$  and  $\rho_L$  are the weight and the density of a liquid phase, and  $W_S$  and  $\rho_S$  are those of a solid phase, respectively.

## 2.2. $^1\text{H}$ NMR and $^1\text{H}$ qNMR measurements

$^1\text{H}$  NMR and  $^1\text{H}$  quantitative NMR (qNMR) spectra were observed on an INOVA 400 (magnetic field strength of 9.39 T) pulse FT-NMR spectrometer (Varian Inc., USA) with a tunable broad-band probe at room temperature. All NMR spectra were recorded at an operating frequency of 399.783 MHz, and were applied a sweep width of 16,000 kHz (40.021 ppm); the data acquisition time was 8.192 s, and the data number during the free induction decay were collected in 262,140 points. The Lorentzian line-broadening factor (i.e. window function) was not applied to the total free induction decay prior to Fourier transformation. The FID scans of 32 times were recorded by applying a 0.02 s recycle delay between  $30^\circ$  pulse sequences which pulse width is 3.6  $\mu\text{s}$  to improve the signal-to-noise ratio and to avoid saturation. It was confirmed that further extension of the relaxation delay did not change the intensity of  $^1\text{H}$  NMR spectra. The gain of the RF amplifier in an NMR spectrometer (i.e., receiver gain) was always constant. The  $^1\text{H}$  NMR chemical shifts were determined against a second order external standard of  $\text{H}_2\text{O}$  in 10%  $\text{D}_2\text{O}$  for 4.790 ppm (tetramethylsilane as a first order standard is

0 ppm). The sample tube spinning was stopped during the measurement because the measurement samples were gelatinous.

$^1\text{H}$  qNMR analysis was carried out using the integrated intensities of  $^1\text{H}$  NMR signals due to PC molecules.  $^1\text{H}$  qNMR is defined as following equation [33,34];

$$\frac{N_x}{N_{\text{ref}}} = T \times 10^{\frac{Rg_{\text{ref}} - Rg_x}{20}} \times \frac{Ns_{\text{ref}}}{Ns_x} \times \frac{I_x}{I_{\text{ref}}} \quad (4)$$

where  $N$  is the concentration of the chemical species which give the NMR signal,  $Rg$  is the receiver gain in decibel unit of an NMR spectrometer (i.e., receiver gain),  $Ns$  is the number of FID scans, and  $I$  is the integrated intensity of the NMR signal. The subscripts “x” and “ref” indicate the sample solution and the external reference for NMR measurements, respectively.  $T$  indicates the specific constant value which is affected by the condition of an entire NMR observation system, e.g. NMR spectrometer, NMR probe, NMR sample tube, etc., and it is almost 1 when a similar NMR sample tube and the same NMR equipment are used for measurements. To assure the accuracy of the integrated intensity of NMR signals, the NMR spectral data after the Fourier transform carefully corrected the phase and the baseline, moreover, the integrated intensity was calculated manually by the sectional measurement method on the Microsoft Excel.

### 2.3. $^1\text{H}$ NMR relaxation time measurements

The  $T_1$  and  $T_2$  of all  $^1\text{H}$  nuclei were determined by the inversion recovery [35] and CPMG procedures, respectively [36], using an Acorn area (magnetic field strength of 0.3 T) as a specialized measuring device measuring of  $^1\text{H}$  NMR relaxation (XiGo Nanotools Inc., USA). The sample was put into 5 mm diameter glass NMR tube. All experiments were performed at  $25 \pm 0.5$  °C. The theoretical spin-lattice and spin-spin NMR relaxations of a nucleus are expressed as following equations;

$$M_{(\tau)} = M_{(0)} \{ 1 - \exp( - \frac{\tau}{T_1} ) \} \quad (5)$$

$$M_{(\tau)} = M_{(0)} \cdot \exp( - \frac{\tau}{T_2} ) \quad (6)$$

where  $M_{(\tau)}$  is  $z$ -magnetization after pulse delay  $\tau$  of the inversion recovery or CPMG procedure. The averaged  $T_1$  and  $T_2$  values of all  $^1\text{H}$  nuclei of PC molecules in a sample solution were obtained in this work.

#### 2.4. Zeta potential and FT-IR spectroscopy measurement

The measurements of zeta potential on the surfaces of FS, FA, and FT nanoparticles were recorded using an ELS-Z2000 (Otsuka Electronics Co., Ltd., Japan) by an electrophoretic light scattering method (i.e., laser Doppler method) at  $25 \pm 0.5$  °C. The solid-liquid coexisting model samples (solid phase: FS, FA, or FT, liquid phase: 0.01 mol L<sup>-1</sup> LiClO<sub>4</sub> PC solution) were prepared in Ar glovebox. The  $\phi_L$  values of the zeta potential measurement samples was prepared high as 99.9 vol% to retain the flowability. After preparation, thus measurement samples were transferred to a quartz glass flow cell and stabilized at  $25 \pm 0.5$  °C. The fumed oxide nanoparticles were uniformly dispersed in a liquid phase inside while the zeta potential measuring. The determined zeta potential values are average values of three times measurements to minimize data errors. FT-IR spectra were measured using Fourier transform-infrared spectrometer (FT-IR; FT/IR-615R JASCO Corp., Japan) with a HgCdTe detector by the resolution of 4 cm<sup>-1</sup>. The measurement was carried out by diffuse reflection method (DR-400, JASCO Corp., Japan).

### 3. Results and discussion

Dependence of the  $^1\text{H}$  NMR of PC molecules (without the fumed oxides) on the LiClO<sub>4</sub> concentration is shown in Fig. 1. As the LiClO<sub>4</sub> concentration increased, the signal peaks gradually



shifted toward low magnetic field because of the decrease in the electron density around the hydrogen nucleus of the PC molecule; this occurred when the  $\text{Li}^+$  ions were solvated by PC through the carbon atom of the carbonyl group in PC. The  $^1\text{H}$  NMR signals show significant broadening when the  $\text{LiClO}_4$  concentration is greater than  $3 \text{ mol L}^{-1}$ . Approximately 11.8 mol of PC molecules exist in 1 L of PC, and the coordination number of PC molecules to the  $\text{Li}^+$  ion is 4 [37–39]. Therefore, the number of free PC molecules (which are not involved in the solvation of  $\text{Li}^+$  ions) decreases drastically when the  $\text{LiClO}_4$  concentration is more than  $3 \text{ mol L}^{-1}$ . When the electrolyte concentration increases above  $3 \text{ mol L}^{-1}$ , the viscosity of the PC solution increases rapidly upon formation of the solvation structure and hydrogen-bonded network, and all the  $^1\text{H}$  NMR signals undergo broadening.

The dependence of the  $^1\text{H}$  NMR spectra of PC molecules (with fumed oxides) on the  $\phi_L$  value is shown in Fig. 2. In the FA/PC and FS/PC systems, the  $^1\text{H}$  NMR signal shifts toward high magnetic field when the  $\phi_L$  value decreases, while the signal gradually shifts toward low magnetic field in the FT/PC system. Thus, the electron density around the  $^1\text{H}$  nuclei in PC molecules increases in the presence of FA or FS and decreases in the presence of FT. Furthermore, regardless of the choice of fumed oxide, the magnitude of the chemical shift appears to be proportional to the decrease in the  $\phi_L$  value. To understand the above-mentioned result more quantitatively, the dependence of the change in the  $^1\text{H}$  NMR chemical shift of PC molecules (with fumed oxides) on the  $\phi_L$  value of PC was studied (Fig. 3). Thus, the proportional relationship between the increase of the solid phase fraction,  $\phi_s$  ( $\phi_s = 1 - \phi_L$ ) (the increase of the total solid surface area), and the change in the electron density around the  $^1\text{H}$  nuclei of the solvent molecule (i.e., changes in  $^1\text{H}$  NMR chemical shift of solvent molecules) is established. The zeta potentials of all the fumed oxides in  $0.01 \text{ mol L}^{-1} \text{ LiClO}_4$  PC solution at  $25 \pm 0.5 \text{ }^\circ\text{C}$  are shown in Table 1. When the solid phase was FA or FS, the  $^1\text{H}$  NMR signals shifted toward higher magnetic fields with increasing  $\phi_s$ . It is considered that the solid phase surface of FA with a large positive zeta potential attracts the PC molecule more strongly by the interaction with the local

negative electric field (caused by polarization) in the PC molecule. As a result, the  $^1\text{H}$  NMR signals due to the solvent PC molecules shift to high magnetic field owing to the strong magnetic shielding effect by the electrons in the solid phase. In the case of FT, which has a larger positive zeta potential than FA, a large shift toward high magnetic field can be expected owing to similar factors. However, in reality, a shift toward low magnetic field was observed with increasing  $\phi_s$  value. This result may be related to the special property of  $\text{TiO}_2$ , namely, the Honda–Fujishima effect [40,41]. The surface of  $\text{TiO}_2$  acquires electron-holes in the valence band upon light irradiation. These electron-holes strongly attract electrons from other substances, and therefore, the charge density near the  $^1\text{H}$  nuclei of PC molecules, which are attracted to the FT surface, decreases. As a result, the  $^1\text{H}$  NMR signals due to the PC molecules shift significantly toward low magnetic field. Since these interactions occur between the solid phase surface and solvent molecules, the change in chemical shift of the PC molecule is proportional to the  $\phi_s$  value.

The changes in the  $^1\text{H}$  NMR spectra of the PC molecule owing to the increase in the  $\phi_s$  value are not limited to NMR chemical shifts. As shown in Fig. 2, all the  $^1\text{H}$  NMR signals due to the PC molecules are remarkably broadened by the introduction of only 1–2 vol% of any of the fumed oxides. The line width of the NMR signals corresponds to the spin–spin relaxation time ( $T_2$ ) of the observed nucleus. Accordingly, variation of  $T_2$  of the  $^1\text{H}$  NMR in electrolyte solutions upon changing the  $\phi_L$  value is shown in Fig. 4. Here, in order to discuss dynamics of solvent molecules in restricted area between dispersed nano solid-particles, we proposed the hexagonal close packing model as shown in Scheme S2 which liquid layer is on solid surface and the solid particles are monodispersed [42]. In this model, it is assumed that the interaction between the solid particles which has the liquid layer can be ignored and they are closely packed. Therefore, the apparent average liquid phase thickness, “ $\ell_L$ ”, can be introduced to quantitatively interpret the relationship between the liquid phase thickness on the solid phase surface and the mobility of the solvent molecules. The  $\ell_L$  value can be derived from the hexagonal close packing model as shown in Scheme S2:

$$t_L = \left[ \left[ \frac{\pi}{3\sqrt{2}(1-\phi_L)} \right]^{1/3} - 1 \right] \cdot r \quad (7)$$

where  $r$  is the average diameter of the primary particle in the solid phase. Upon comparison with the PC solution system, it is obvious that the decrease of  $T_2$  with the increase of  $\phi_s$  is significant for the aqueous solution system. The  $T_2$  values of water molecule are significantly lower in the presence of only 0.5–1 vol% of the solid phase. At this time,  $t_L$  is 15–40 nm, which corresponds to the length of 40–100 water molecules.

The NMR relaxation times,  $T_1$  and  $T_2$ , because of the dipole–dipole relaxation mechanism of a dipolar nucleus (e.g.,  $^1\text{H}$ ) can be theoretically expressed in the region of extreme narrowing (i.e., the region in which  $T_2$  is almost equal to the spin–lattice relaxation time,  $T_1$ ) as follows [30,43]:

$$T_1 = T_2 = \frac{d^6}{10a\gamma^4\tau_c} \quad (8)$$

where  $a = 3\mu_0^2\hbar^2/320\pi^2$ ,  $\mu_0$  is the permeability of vacuum,  $d$  is the distance between the nuclei,  $\gamma$  is their gyromagnetic ratio, and  $\tau_c$  is the rotational correlation time of a spherical molecule rotating in a liquid. The mobility of water molecules in the vicinity of the solid-phase surface lowers (namely, the  $\tau_c$  of water molecule increases) because of hydrogen bonding to the surface; as a consequence, the  $T_2$  of the water molecule is expected to decrease. In contrast, in case of the FS–PC solution coexisting system, the decrease of  $T_2$  accompanying the increase in the solid phase fraction is not as pronounced as seen in the aqueous solution system (Fig. 4(b)). This suggests that the interaction between the PC molecule and the solid phase surface is relatively weak and the mobility of PC molecules is less limited by the presence of solid phase than that of water molecules. The zeta potentials of all the fumed oxides in 0.01 mol L<sup>-1</sup> LiClO<sub>4</sub> PC solution at 25 ± 0.5 °C are shown in Table 1. FS, which has the smallest absolute

value of zeta potential, is expected to have the least electrostatic interactions with solvent PC molecules. In fact, the decrease of  $T_2$  upon increase of  $\phi_s$  is the lowest when the solid phase is FS. Thus, the  $T_2$  values due to the PC molecule depend on the solid phase fraction in the order  $FA > FT > FS$ . However, there is no good correlation between this order and the surface zeta potential of these solid phases. This may be attributed to the fact that the specific surface area of FT ( $90 \pm 20 \text{ m}^2 \text{ g}^{-1}$ ) is lesser than that of FS ( $200 \pm 25 \text{ m}^2 \text{ g}^{-1}$ ) and FA ( $130 \pm 20 \text{ m}^2 \text{ g}^{-1}$ ). Furthermore, as another reason, owing to the counter anion condensation to the solid surface of FA and FT and the electric double layer, the magnitude of the effective electric field which electrostatically affects solvent molecules may be different from the order of the zeta potential. In the case of the FA–PC solution coexisting system, as with water molecules, the  $T_2$  values due to the PC molecules decreased because of the presence of only 0.5–1 vol% of the solid phase (i.e., the  $t_L$  is 15–40 nm). Furthermore, the concentration dependence of  $\text{LiClO}_4$  as the electrolyte is more pronounced in the PC solution system than in the aqueous system, and this is as attributed to the influence of the viscosity of the liquid phase. Namely, in a  $1 \text{ mol L}^{-1} \text{ LiClO}_4$  aqueous solution, about 53 mol of water molecules exist per 1 mol of  $\text{Li}^+$  ions in 1 L of the solution; hence, only a small fraction of the water molecules are involved in the hydration of the  $\text{Li}^+$  ions. Therefore, even if the  $\text{Li}^+$  ion concentration increases, the hydrogen bond network in the solvent is stable and the increase in viscosity is relatively small. In contrast, in a  $1 \text{ mol L}^{-1} \text{ LiClO}_4$  PC solution, there are only 11 mol of PC molecules per 1 mol of  $\text{Li}^+$  ions in 1 L of the solution; thus, the proportion of PC molecules, which are involved in solvation is higher than that in the aqueous solution. Consequently, when the electrolyte concentration increases in the PC solution, the viscosity of the solution increases significantly owing to the rapid development of the solvation structure and hydrogen bonding network. As a result, in the PC solution system, the  $T_2$  decreases with the increase of electrolyte concentration regardless of the  $\phi$  value for all the solid phases (FS, FA, and FT). The solid phase surface is considered to have little influence on the solvation structure and hydrogen bond network.

Comparing  $T_1$  and  $T_2$  can yield information concerning the mobility of the observed chemical species. For two identical dipolar nuclei existing in the same molecule, the intramolecular dipole–dipole relaxation times are given by the following equations [30–32,43]:

$$T_1 = \frac{d^6}{2a\gamma^4 \left( \frac{\tau_c}{1+\omega^2\tau_c^2} + \frac{4\tau_c}{1+4\omega^2\tau_c^2} \right)} \quad (9)$$

$$T_2 = \frac{d^6}{a\gamma^4 \left( 3\tau_c + \frac{5\tau_c}{1+\omega^2\tau_c^2} + \frac{2\tau_c}{1+4\omega^2\tau_c^2} \right)} \quad (10)$$

where  $\omega$  is the angular velocity of Larmor precession motion of the nucleus in the external magnetic field, that is, the angular frequency of the radio wave used for NMR observation. When  $\omega\tau_c < 1$ , this is known as the “extreme narrowing region,” and  $T_1$  and  $T_2$  are almost equal [30,32,43]. However, if the mobility of the molecule decreases and  $\omega\tau_c$  becomes greater than unity because of the increase of  $\tau_c$ , then  $T_1 > T_2$ . The correlation between  $T_1$  and  $T_2$  of  $^1\text{H}$  NMR due to  $\text{H}_2\text{O}$  or PC molecules in the FS + C mol L<sup>-1</sup> LiClO<sub>4</sub> aqueous or PC solution systems ( $C = 0\text{--}3$ ) is shown in Fig. 5 (The dependence of  $T_1$  of  $^1\text{H}$  NMR ( $\text{H}_2\text{O}$  or PC molecule) on  $\phi_L$  in the solutions is shown in Fig. S1). In the aqueous solution system, the difference between  $T_1$  and  $T_2$  is relatively small although  $T_1 > T_2$  when the  $\phi_L$  value is sufficiently high (i.e., 99.5 vol% or more, closed symbols in Fig. 5) and water molecules move almost freely. However, if the  $\phi_L$  value decreases below 99.5 vol% (i.e., open symbols in Fig. 5), the water molecules in the vicinity of the solid phase surface are strongly hydrogen bonded to it, so that the mobility of water molecules decreases and  $T_1 \gg T_2$  is observed. Moreover, significant electrolyte concentration dependence is not observed, and these results support the discussion of Fig. 4. Hence, the following results can be confirmed for the PC solution system:

1. As the electrolyte concentration increases,  $T_1$  and  $T_2$  decrease significantly. With increasing electrolyte concentration, the viscosity of the PC solution increases remarkably owing to the rapid development of the solvation structure and growth of the hydrogen bond network.
2. Regardless of the increase in electrolyte concentration, the difference between  $T_1$  and  $T_2$  is relatively small when the  $\phi_L$  value is sufficiently high (i.e., 99.5 vol% or greater). The increase in the solution viscosity accompanying an increase in the electrolyte concentration does not significantly lower the mobility of the molecules.
3. In the case of an increase in the  $\phi_S$  value rather than an increase in the electrolyte concentration,  $T_1$  becomes much larger than  $T_2$ . The existence of a solid phase reduces the mobility of the molecule and the interaction between the solid phase surface and the solvent PC molecules greatly affects their mobility.

The above discussion shows that, in order to realize an electrolyte solution with high ionic conductivity, high electrolyte (i.e., ion carrier) concentration is important along with the choice of a solvent that shows weak interactions with the solid phase surface.

Fig. 6 shows the dependence of the  $^1\text{H}$  NMR detection ratios (of  $\text{H}_2\text{O}$  or PC molecules) on the  $\phi_L$  value. The dotted lines in Fig. 6 show the case which all solvent molecules present in the samples were detected by  $^1\text{H}$  NMR. If the mobility of solvent molecules in the sample is lowered drastically because of ion solvation or interaction with a solid phase surface,  $T_2$  will be significantly reduced (i.e., the NMR signal will broaden) and  $T_1$  will increase markedly. In this case, the detection of solvent molecules becomes practically impossible in solution NMR. In the aqueous solution system (Fig. 6(a)), the decrease in the  $^1\text{H}$  NMR detection ratio due to the solvent water molecules is caused by two factors: (1) increase in the electrolyte concentration, and (2) increase in the  $\phi_S$  value. In particular, the influence

of the increase in the electrolyte concentration was remarkable and the  $^1\text{H}$  NMR detection ratio of the water molecule was greatly reduced by the increase in electrolyte concentration, even in the absence of the solid phase ( $\phi_L = 100$  vol%). In the case of structure-forming ions such as  $\text{Li}^+$ , the water molecules are strongly attracted to the ions and form an orderly structure; these water molecules are extremely hard to move compared to bulk water molecules. In contrast, the decrease in the  $^1\text{H}$  NMR detection ratio of water molecules because of the increase of the  $\phi_S$  value is small. Although the  $^1\text{H}$  NMR detection ratio of water molecules decreases slightly because of an increase in the solid phase of about 0.5–1 vol%, it is obvious that 1 vol% or more of the solid phase has little influence on the mobility of the water molecules. Furthermore, the decrease in the  $^1\text{H}$  NMR detection ratio of PC molecules is mainly caused by the increase in the  $\phi_S$  value. When the solid phase is FS, which has the smallest absolute value of the surface zeta potential, the decrease in the  $^1\text{H}$  NMR detection ratio because of the increase in the  $\phi_S$  value is the least, and the electrostatic interaction with solvent PC molecules is considered to be the smallest. This is consistent with the result of the smallest  $\phi_S$  value dependence of  $T_2$  when the solid phase is FS (Fig. 4). The order of dependence of the  $^1\text{H}$  NMR detection ratio of PC solvent on the  $\phi_S$  value is  $\text{FA} > \text{FT} > \text{FS}$ . This order is consistent with the solid phase fraction dependence of  $T_2$ , as shown in Fig. 4, and the strength of the interaction between the solid phase surface and the PC molecule also follows this trend. In the case of an aqueous solution system, the pH dependence of the zeta potential and the point of zero charge (i.e., PZC) of carbon black powder which is applied as a conductive material in composite electrodes for secondary batteries are similar to those of  $\alpha\text{-Al}_2\text{O}_3$ . [44,45] Therefore, it is expected that the influence on the physical properties of a solvent by the mixture of carbon black powder to an electrolyte solution is similar to that if  $\alpha\text{-Al}_2\text{O}_3$  is added to the electrolyte solution .

The FT–IR spectra due to the C=O stretching vibration of the PC molecule at low  $\phi_L$  values (i.e.,  $\phi_L < 75$  vol%) are shown in Fig. 7. The interaction between the PC molecules and the solid phase

surface affects the wave number of the C=O stretching vibration. When intermolecular interactions occur, the wave number shifts; as a result, the absorption band generally widens and can exhibit a split peak. If the solid phase is not included ( $\phi_L = 100$  vol%), the C=O stretching vibration is observed (Fig. 7) as a single peak at  $1780\text{ cm}^{-1}$  [46], and in the case of the solid–liquid coexisting system, the peak splits into two peaks, namely the peaks in lower and higher wavenumber regions. From the general empirical rule, the peak in lower wavenumber is the C=O stretching vibration of the PC molecules which contain the interactions between the C=O groups and the solid phase. In addition, it can be considered that the peak in higher wavenumber is that of the PC molecules which contain the interactions between the hydrocarbon groups and the solid phase. Focusing on the peak in the lower wavenumber, it can be seen that the PC molecule peak in FS occurs at  $1770\text{ cm}^{-1}$ , while it appears in the vicinity of  $1730\text{ cm}^{-1}$  in FA and FT. Hence, it can be confirmed that the interaction between the PC molecule and the solid phase surface is weakest in FS. This is in agreement with the results of the  $^1\text{H}$  NMR chemical shift change and relaxation time studies. This peak splitting is most noticeable at  $\phi_L = 75$  vol% and obscures at  $\phi_L = 50$  vol%. When  $\phi_L \geq 75$  vol%, one PC molecule interacts with the surface of one particle because of the small  $\phi_s$  value. However, at  $\phi_L \leq 50$  vol%, each PC molecule interacts intricately with the surface of multiple particles increasing the diversity of the C=O stretching vibration, making the peak split obscure. In this case, it is presumed that the mobility of the PC molecule is severely limited. On the other hand, in the case of the peak in the higher wavenumber, the electron-withdrawing property of the oxygen atom adjacent to the C=O group increases due to the solid phase electron which brought a higher magnetic field shift of the  $^1\text{H}$  NMR signal (Fig. 3) of the hydrocarbon group in PC molecule, and as a result the IR signals of the C=O groups shift towards the high wavenumber region. It can be estimated that this tendency is remarkable if the solid phase is FS and FA.

#### 4. Conclusions



The non-aqueous  $\text{LiClO}_4$  solutions kneaded with FS, FA, and FT were employed as model systems of lithium ion batteries. The proportional relationship between the  $\phi_s$  values and  $^1\text{H}$  NMR chemical shift changes in  $^1\text{H}$  NMR chemical shift of solvent molecules, namely, in the electron density around the  $^1\text{H}$  nuclei of the solvent molecule was established. The solid phase surface of fumed oxides attracted strongly the PC molecule by the interaction with local negative electric field which caused by polarization in PC molecule. These interactions occurred between the solid phase surface and solvent molecules, the chemical shift change amount of the PC molecule was proportional to the solid phase fraction. The decrease of  $T_2$  according to the increase of the solid phase fraction was remarkable for the FS-aqueous solution coexisting system. The  $T_2$  values of water molecule were significantly lower in the presence of the solid phase when  $t_L$  is 15 to 40 nm (i.e., the length of 40 to 100 water molecules) because of the decrease of mobility by the strong hydrogen bonding to solid surface. The decrease of  $T_2$  accompanying the increase in the solid phase fraction was not as pronounced as seen in the aqueous solution system for the FS-PC solution coexisting system because the interaction between the PC molecule and the solid phase surface is relatively weak. In the case of PC solution, the viscosity of the solution remarkably increased owing to the rapid development of the solvation structure and hydrogen bonding network according to the increasing of the electrolyte concentration. Therefore the concentration dependency of  $\text{LiClO}_4$  as the electrolyte was more pronounced in the PC solution system and the solid phase surface had little influence on the developed solvation structure and hydrogen bond network. The following results could be confirmed for the PC solution system by the comparing  $T_1$  and  $T_2$ : (i) the viscosity of the PC solution increases remarkably owing to the rapid development of the solvation structure and growth of the hydrogen bond network with the increasing electrolyte concentration, (ii) the increase in the solution viscosity accompanying an increase in the electrolyte concentration did not significantly lower the mobility of the molecule, and (iii) the existence of a solid phase reduced the mobility of the molecule and the interaction between the solid phase surface and the solvent PC molecules greatly affected their mobility. The decrease in the  $^1\text{H}$  NMR detection ratio of PC

molecules was mainly caused by the increase in the solid phase fraction, and order of dependence of the  $^1\text{H}$  NMR detection ratio of PC solvent on the  $\phi_s$  value is  $\text{FA} > \text{FT} > \text{FS}$ . This order was consistent with the  $\phi_s$  dependence of  $T_2$ , and the strength of the interaction between the solid phase surface and the PC molecule also follows this trend.

## Acknowledgment

This study is supported by the research project of No.12101607 in "Phase Interface Science for Highly Efficient Energy Utilization" of JST Core Research for Evolutional Science and Technology (CREST). We would like to thank Professor Takeshi Abe and their colleagues. The FS, FA, and FT samples used as solid phases were kindly gifted from NIPPON AEROSIL Co. Ltd., Japan.

## References

- [1] M. V. Fedorov, A. A. Kornyshev, Ionic Liquids at Electrified Interfaces, *Chem. Rev.* 114 (2014) 2978–3036.
- [2] M. Watanabe, M. L. Thomas, S. Zhang, K. Ueno, T. Yasuda, K. Dokko, Application of Ionic Liquids to Energy Storage and Conversion Materials and Devices, *Chem. Rev.* 117 (2017) 7190–7239.
- [3] J. Huang, Generalization of Porous Electrode Theory for Noninteger Dimensional Space, *J. Phys. Chem. C* 122 (2018) 557–565.
- [4] M. Mizuhata, H. Ikeda, A. Kajinami S. Deki, Effect of solid surface on vibrational modes of solution in solid/liquid hetero-phase system, *J. Mol. Liq.* 83 (1999) 179–189.
- [5] S. Deki, A. Kajinami, Y. Kanaji, M. Mizuhata, K. Nagata, Properties of  $\text{CaCl}_2$  hydrate with an inorganic powder. Part 2.—Melting behaviour and thermodynamic properties of  $\text{CaCl}_2 \cdot n\text{H}_2\text{O}$  ( $n=6.00\text{--}7.35$ ) with  $\alpha\text{-Al}_2\text{O}_3$  or  $\alpha\text{-SiC}$  powder, *J. Chem. Soc. Faraday Trans.* 89 (1993) 3811–3815.
- [6] A. B. Béléké, M. Mizuhata, S. Deki, Vib. Anomalous properties of molten alkali nitrates coexisting with aluminum oxides by hetero-phase effect, *Spectrosc.* 40 (2006) 66–79.
- [7] S. Deki, S. Nakamura, A. Kajinami, Y. Kanaji, M. Mizuhata, Properties of  $\text{CaCl}_2$  hydrate with an inorganic powder. Part 1.—Electrical conductivity of  $\text{CaCl}_2 \cdot n\text{H}_2\text{O}$  ( $n=6.00\text{--}7.35$ ) with  $\alpha\text{-Al}_2\text{O}_3$  powder, *J. Chem. Soc. Faraday Trans.* 89 (1993) 3805–3810.
- [8] S. Deki, M. Mizuhata, S. Rakuno, A. Kajinami, Electrical Conductivity of Solid/Liquid Coexisting Systems: Dependence of Electrical Conductivity on Surface Hydrophilicity, *J. Colloid Interface Sci.* 168 (1994) 198–205.
- [9] T. Ohkubo, T. Konishi, Y. Hattori, T. Fujikawa, K. Kaneko, Restricted Hydration Structures of Rb and Br Ions Confined in Slit-Shaped Carbon Nanospace, *J. Am. Chem. Soc.* 124 (2002) 11860–11861.

- [10] S. Jähnert, F. V. Chávez, G. E. Schaumann, A. Schreiber, M. Schönhoff, G. H. Findenegg, Melting and freezing of water in cylindrical silica nanopores, *Phys. Chem. Chem. Phys.* 10 (2008) 6039–6051.
- [11] M. Mizuhata, M. Kitamura, S. Deki, Nano-pore Effect on Ionic Conduction of Non-aqueous  $\text{LiClO}_4$  Solution Coexisting with Porous Solid Materials, *Electrochemistry* 71 (2003) 1093–1095.
- [12] K. Xu, Electrolytes and Interphases in Li-Ion Batteries and Beyond, *Chem. Rev.* 114 (2014) 11503–11618.
- [13] W. Li, J. R. Dahn, D. S. Wainwright, Rechargeable Lithium Batteries with Aqueous Electrolytes, *Science* 264 (1994) 1115–1118.
- [14] C. Wessells, R. Ruff, R. A. Huggins Y. Cui, Electrochem. Investigations of the Electrochemical Stability of Aqueous Electrolytes for Lithium Battery Applications, *Solid-State Lett.* 13 (2010) A59–A61.
- [15] W. R. Fawcett, P. J. Ryan, T. G. Smagala, Properties of the Diffuse Double Layer at High Electrolyte Concentrations, *J. Phys. Chem. B* 113 (2009) 14310–14314.
- [16] X-R. Liu, L. Wang, L-J. Wan, D. Wang, In Situ Observation of Electrolyte-Concentration-Dependent Solid Electrolyte Interphase on Graphite in Dimethyl Sulfoxide, *ACS Appl. Mater. Interfaces* 7 (2015) 9573–9580.
- [17] J. H. Bae, C. M. Kang, H. Choi, B. J. Kim, W. Jang, S. Y. Lim, H. C. Kim T. D. Chung, Nonfaradaic Nanoporous Electrochemistry for Conductometry at High Electrolyte Concentration, *Anal. Chem.* 87 (2015) 2443–2451.
- [18] Y. Yamada, K. Furukawa, K. Sodeyama, K. Kikuchi, M. Yaegashi, Y. Tateyama, A. Yamada, Unusual Stability of Acetonitrile-Based Superconcentrated Electrolytes for Fast-Charging Lithium-Ion Batteries, *J. Am. Chem. Soc.* 136 (2014) 5039–5046.

- [19] M. Mizuhata, Y. Sumihiro, S. Deki, Structure and the conductive behaviour of hydrate melt coexisting with porous solid materials— $\alpha$ - $\text{Al}_2\text{O}_3$  powder/ $\text{ZnCl}_2$  hydrate melt coexisting system, *Phys. Chem. Chem. Phys.* 6 (2004) 1944–1951.
- [20] M. R. Landry, Thermoporometry by differential scanning calorimetry: experimental considerations and applications, *Thermochim. Acta* 433 (2005) 27–50.
- [21] F. Rull, Structural investigation of water and aqueous solutions by Raman spectroscopy, *Pure Appl. Chem.* 74 (2002) 1859–1870.
- [22] Q. Sun, C. Qin, Raman OH stretching band of water as an internal standard to determine carbonate concentrations, *Chem. Geol.* 283 (2011) 274–278.
- [23] G. E. Walrafen, Raman Spectral Studies of the Effects of Temperature on Water and Electrolyte Solutions, *J. Chem. Phys.* 44 (1966) 1546–1558.
- [24] G. E. Walrafen, Raman Spectral Studies of Water Structure, *J. Chem. Phys.* 40 (1964) 3249–3257.
- [25] H. Thompson, A. K. Soper, M. A. Ricci, F. Bruni, N. T. Skipper, The Three-Dimensional Structure of Water Confined in Nanoporous Vycor Glass, *J. Phys. Chem. B* 111 (2007) 5610–5620.
- [26] P. Smirnov, T. Yamaguchi, S. Kittaka, S. Takahara, Y. Kuroda, X-ray Diffraction Study of Water Confined in Mesoporous MCM-41 Materials over a Temperature Range of 223–298 K, *J. Phys. Chem. B* 104 (2000) 5498–5504.
- [27] P. Porion, A. M. Faugère, A. Delville, Structural and Dynamical Properties of Water Molecules Confined within Clay Sediments Probed by Deuterium NMR Spectroscopy, Multiquanta Relaxometry, and Two-Time Stimulated Echo Attenuation, *J. Phys. Chem. C* 118 (2014) 20429–20444.
- [28] B. Grünberg, T. Emmler, E. Gedat, I. Shenderovich, G. H. Findenegg, H.-H. Limbach, G. Buntkowsky, Hydrogen Bonding of Water Confined in Mesoporous Silica MCM-41 and SBA-15 Studied by  $^1\text{H}$  Solid-State NMR, *Chem. Eur. J.* 10 (2004) 5689–5696.

- [29] A. Vyalikh, Th. Emmeler, B. Grünberg, Y. Xu, I. Shenderovich, G. H. Findenegg, H.-H. Limbach, G. Buntkowsky, Hydrogen Bonding of Water Confined in Controlled-Pore Glass 10-75 Studied by  $^1\text{H}$ -Solid State NMR, *Z. Phys. Chem.* 221 (2007) 155–168.
- [30] J. W. Akitt, *NMR and Chemistry: An Introduction to Modern NMR Spectroscopy*, third ed., Chapman & Hall, London, 1992 (Chapter 4.2).
- [31] W. R. Carper, C. E. Keller, Direct Determination of NMR Correlation Times from Spin-Lattice and Spin-Spin Relaxation Times, *J. Phys. Chem. A* 101 (1997) 3246–3250.
- [32] A. Abragam, *Principles of Nuclear Magnetism*, Oxford University Press, Oxford, U.K., 1961 (Chapter 8).
- [33] H. Maki, Y. Okumura, H. Ikuta, M. Mizuhata, Ionic Equilibria for Synthesis of  $\text{TiO}_2$  Thin Films by the Liquid-Phase Deposition, *J. Phys. Chem. C* 118 (2014) 11964–11974.
- [34] H. Maki, G. Sakata, M. Mizuhata, Quantitative NMR of quadrupolar nucleus as a novel analytical method: hydrolysis behaviour analysis of aluminum ion, *Analyst* 142 (2017) 1790–1799
- [35] R. L. Vold, J. S. Waugh, M. P. Klein, D. E. Phelps, Measurement of Spin Relaxation in Complex Systems, *J. Chem. Phys.* 48 (1968) 3831–3832.
- [36] S. Meiboom, D. Gill, Modified Spin - Echo Method for Measuring Nuclear Relaxation Times, *Rev. Sci. Instrum.* 29 (1958) 688–691.
- [37] H. Ohtaki, T. Radnai, Structure and dynamics of hydrated ions, *Chem. Rev.* 93 (1993) 1157–1204.
- [38] Y. Suwannachot, S. Hannongbua, B. M. Rode, Solvation of lithium chloride in water–hydroxylamine mixtures: A theoretical investigation by means of Monte Carlo simulations, *J. Chem. Phys.* 102 (1995) 7602–7609.
- [39] A. P. Lyubartsev, K. Laasonen, A. Laaksonen, Hydration of  $\text{Li}^+$  ion. An *ab initio* molecular dynamics simulation, *J. Chem. Phys.* 114 (2001) 3120–3126.

- [40] N. Sakai, A. Fujishima, T. Watanabe, K. Hashimoto, Enhancement of the Photoinduced Hydrophilic Conversion Rate of TiO<sub>2</sub> Film Electrode Surfaces by Anodic Polarization, *J. Phys. Chem. B* 105 (2001) 3023–3026.
- [41] N. Sakai, A. Fujishima, T. Watanabe, K. Hashimoto, Quantitative Evaluation of the Photoinduced Hydrophilic Conversion Properties of TiO<sub>2</sub> Thin Film Surfaces by the Reciprocal of Contact Angle, *J. Phys. Chem. B* 107 (2003) 1028–1035.
- [42] N. Kunikata, M. Matsui, H. Maki, M. Mizuhata, Properties of Concentrated Aqueous Electrolyte Solution in a Vicinal Region of Coexisting Solid Surface, *ECS Trans.* 80 (2017) 1459-1470.
- [43] I. Solomon, Relaxation Processes in a System of Two Spins, *Phys. Rev.* 99 (1955) 559–565.
- [44] M. Kosmulski, P. Dahlsten, P. Próchniak, J. B. Rosenholm, Electrokinetics at high ionic strengths: Alumina, *Colloids Surf., A* 301 (2007) 425–431.
- [45] H. Sis, M. Birinci, Effect of nonionic and ionic surfactants on zeta potential and dispersion properties of carbon black powders, *Colloids Surf., A* 341 (2009) 60–67.
- [46] P. A. Brooksby, W. R. Fawcett, Infrared (attenuated total reflection) study of propylene carbonate solutions containing lithium and sodium perchlorate, *Spectrochim. Acta, Part A*, 64 (2006) 372–382.

## Table

Table 1. Zeta potentials of all fumed oxides in 0.01 mol L<sup>-1</sup> LiClO<sub>4</sub> PC solution at 25 ± 0.5 °C. All values were determined by an electrophoretic light scattering method (i.e., laser Doppler method), and they are average values of three times measurements to minimize data errors.

	Fumed silica (FS)	Fumed alumina (FA)	Fumed titania (FT)
	AEROSIL®	AEROXIDE®	AEROXIDE®
	200CF	Alu 130	TiO <sub>2</sub> P 90
Zeta potential (mV)	-1.7	+22.2	+38.7



## Figure captions

Fig. 1.  $\text{LiClO}_4$  concentration dependences of  $^1\text{H}$  NMR spectra of PC molecules without fumed oxides. All peak height is not normalized.

Fig. 2.  $\phi_L$  dependences of  $^1\text{H}$  NMR spectra of PC molecules with fumed oxides. Solid phase: (a) FS (fumed silica), (b) FA (fumed alumina), (c) FT (fumed titania). All measurement samples does not contain any electrolyte. All peak height is not normalized.

Fig. 3. Dependences of the  $^1\text{H}$  NMR chemical shift changes of PC molecules on the  $\phi_L$  value of PC with fumed oxides. NMR chemical shift changes due to the  $^1\text{H}$  nuclei which are circled in the structural formula of PC molecule are shown. The measurement samples does not contain any electrolyte.

Fig. 4.  $\phi_L$  dependences of the spin-spin relaxation time,  $T_2$ , of  $^1\text{H}$  NMR due to  $\text{H}_2\text{O}$  or PC molecule in electrolyte solutions. (a) FS +  $C$  mol/L  $\text{LiClO}_4$  aqueous systems ( $C = 0-3$ ), (b) FS +  $C$  mol/L  $\text{LiClO}_4$  PC solution systems ( $C = 0-3$ ), (c) FA +  $C$  mol/L  $\text{LiClO}_4$  PC solution systems ( $C = 0-3$ ), (d) FT +  $C$  mol/L  $\text{LiClO}_4$  PC solution systems ( $C = 0-3$ ).

Fig. 5. Correlation between the spin-spin relaxation time,  $T_2$ , and the spin-lattice relaxation time,  $T_1$ , of  $^1\text{H}$  NMR due to  $\text{H}_2\text{O}$  or PC molecule in the FS +  $C$  mol/L  $\text{LiClO}_4$  aqueous or PC solution systems ( $C = 0-3$ ). Solid straight line shows the relationship of " $T_2 = T_1$ ". (a) Aqueous solution, (b) PC solution. Open symbols; the data for  $\phi_L < 99.5$  vol% samples, closed symbols; the data for  $\phi_L > 99.5$  vol% samples.

Fig. 6.  $\phi_L$  dependences of the  $^1\text{H}$  NMR detection ratios of  $\text{H}_2\text{O}$  or PC molecule. The  $^1\text{H}$  NMR detection ratios were determined by the ratio of the overall signal integral intensity due to  $\text{H}_2\text{O}$  or PC molecule in the measurement samples without solid phase ( $I$ ) and that with solid phase ( $I_{\text{liquid}}$ ). (a) FS +  $C$  mol/L  $\text{LiClO}_4$  aqueous systems ( $C = 0-3$ ), (b) FS +  $C$  mol/L  $\text{LiClO}_4$  PC solution systems ( $C = 0-3$ ), (c) FA +  $C$  mol/L  $\text{LiClO}_4$  PC solution systems ( $C = 0-3$ ), (d) FT +  $C$  mol/L  $\text{LiClO}_4$  PC solution systems ( $C = 0-3$ ). The dotted lines show the case which all solvent molecules present in the samples were detected by  $^1\text{H}$  NMR.

Fig. 7. FT-IR spectra due to  $\text{C}=\text{O}$  stretching vibration of PC molecule in low  $\phi_L$  value ( $\phi_L < 75$  vol%). PC molecules with fumed oxides. Solid phase: (a) FS, (b) FA, (c) FT. All measurement samples does not contain any electrolyte.

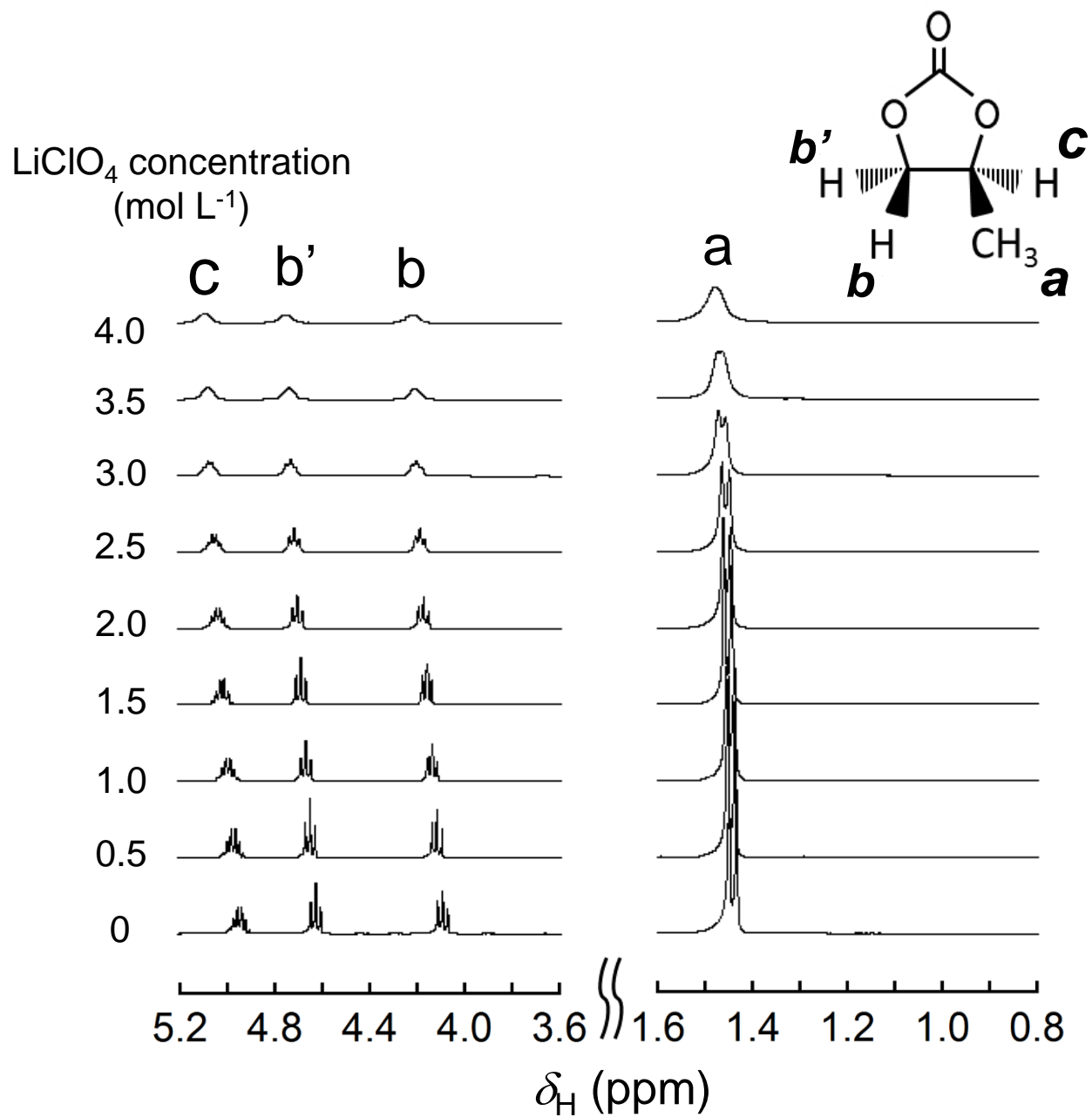


Figure 1

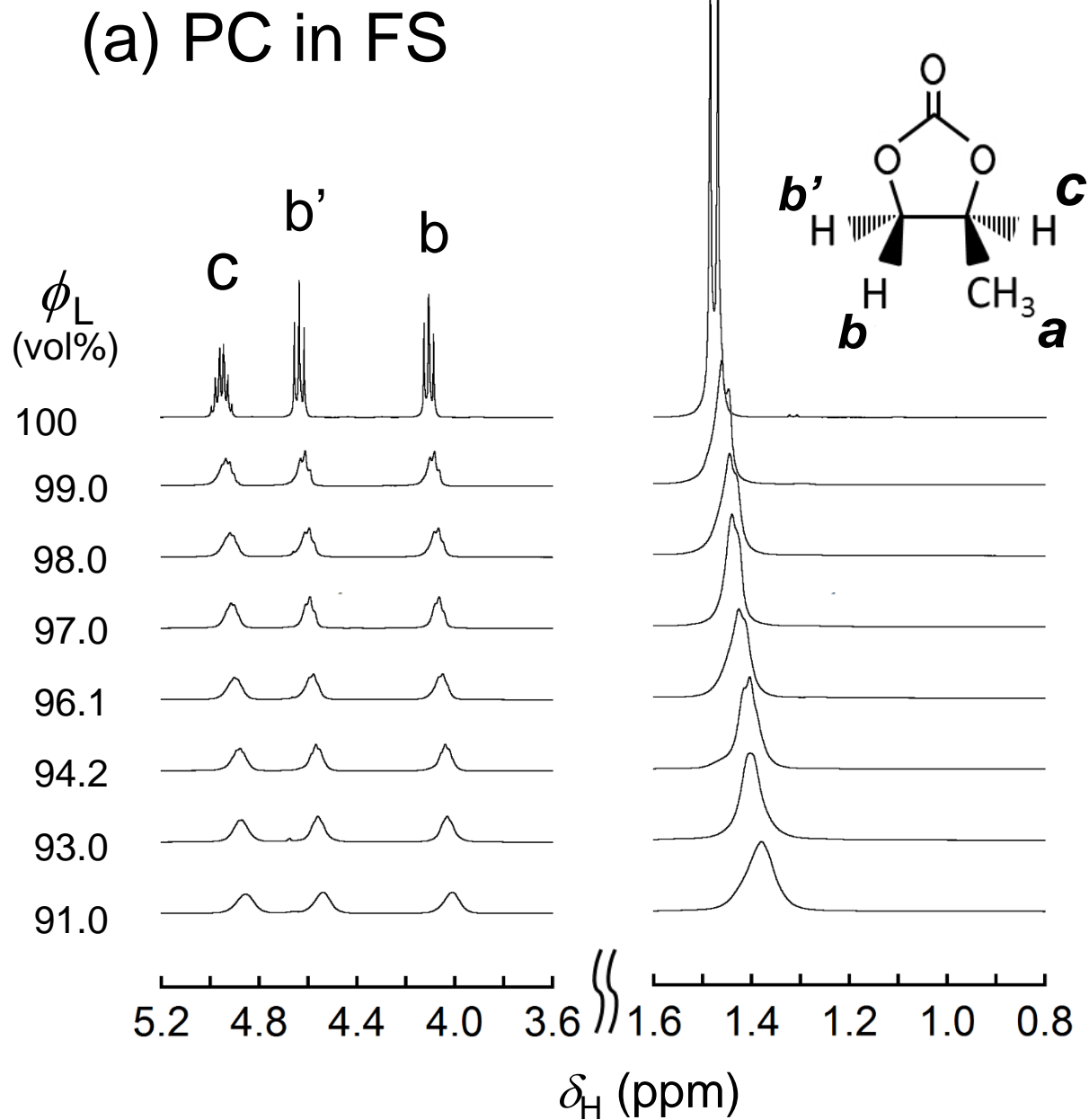


Figure 2(a)

## (b) PC in FA

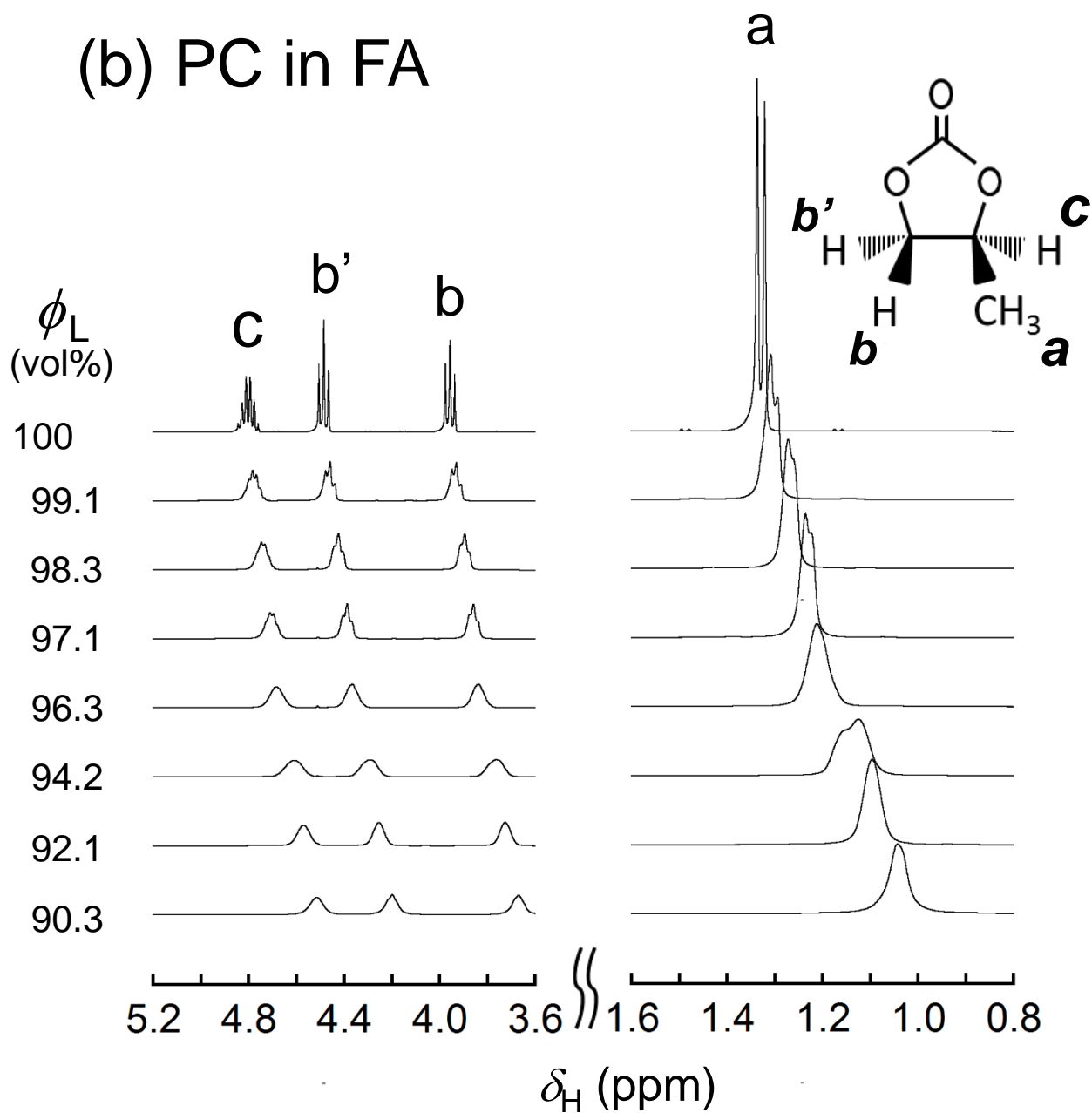


Figure 2(b)

(c) PC in FT

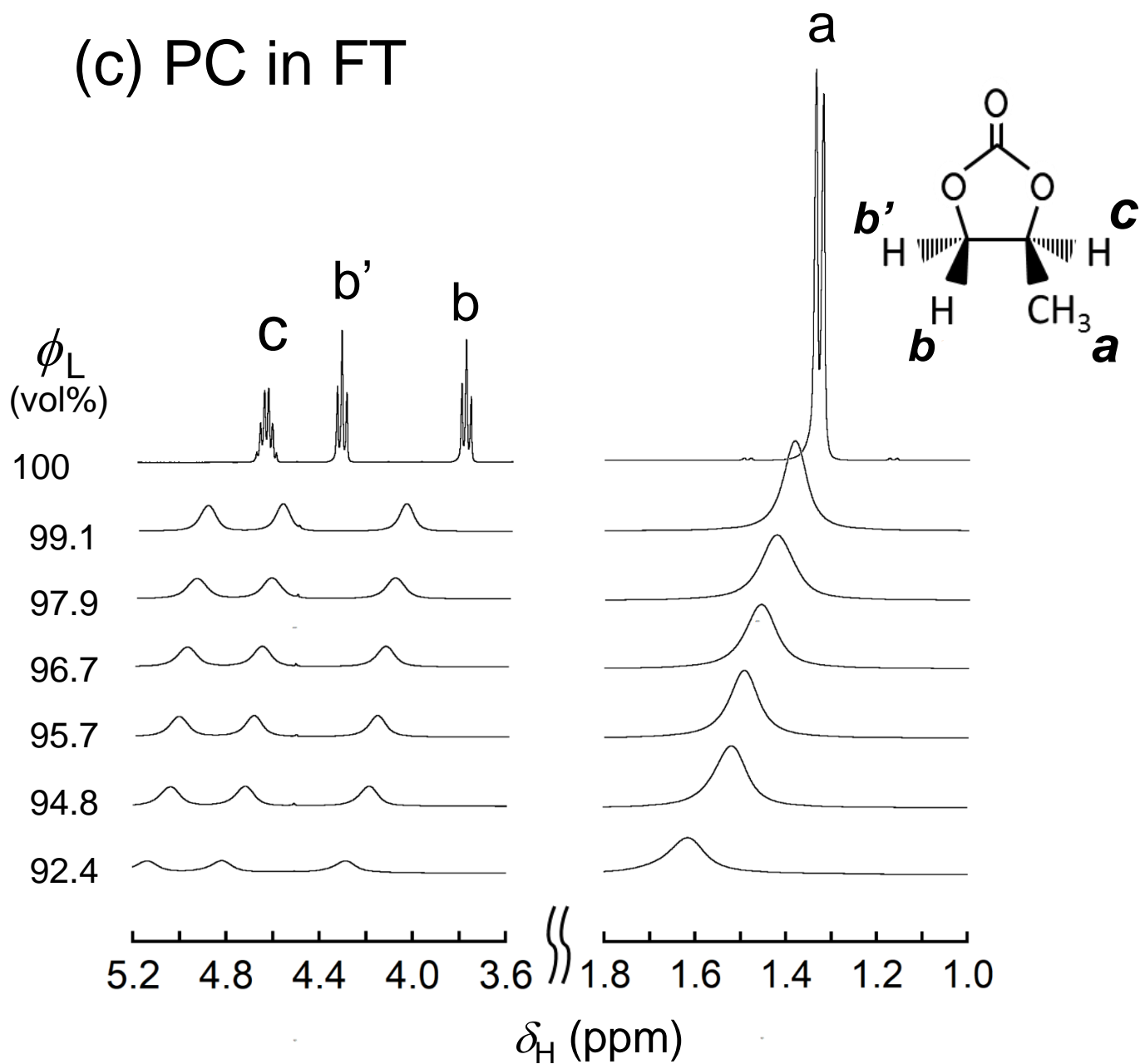


Figure 2(c)

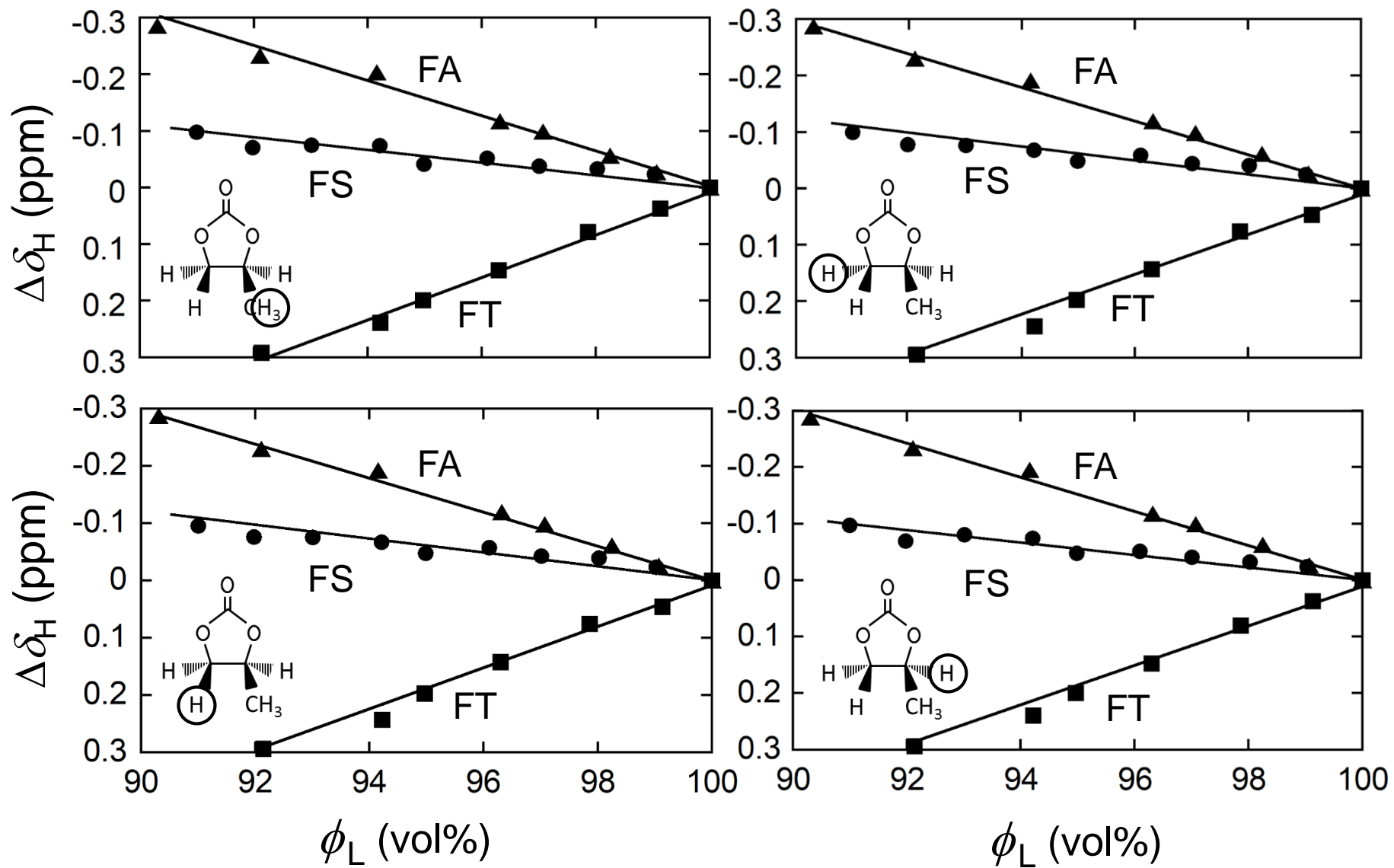


Figure 3

(a) FS +  $C \text{ mol L}^{-1} \text{ LiClO}_4$  aqueous solutions

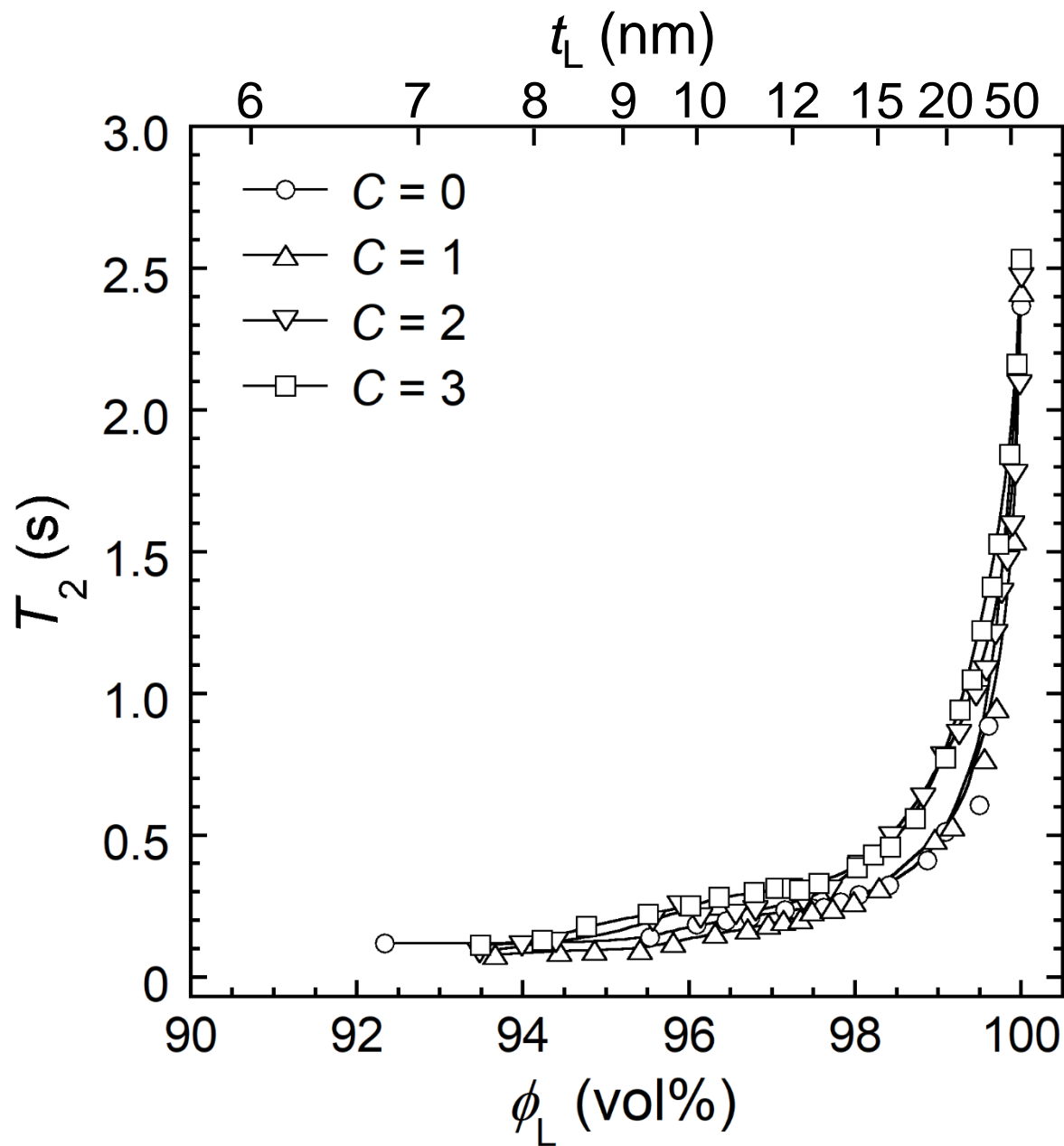


Figure 4(a)



(b) FS + C mol L<sup>-1</sup> LiClO<sub>4</sub> PC solutions

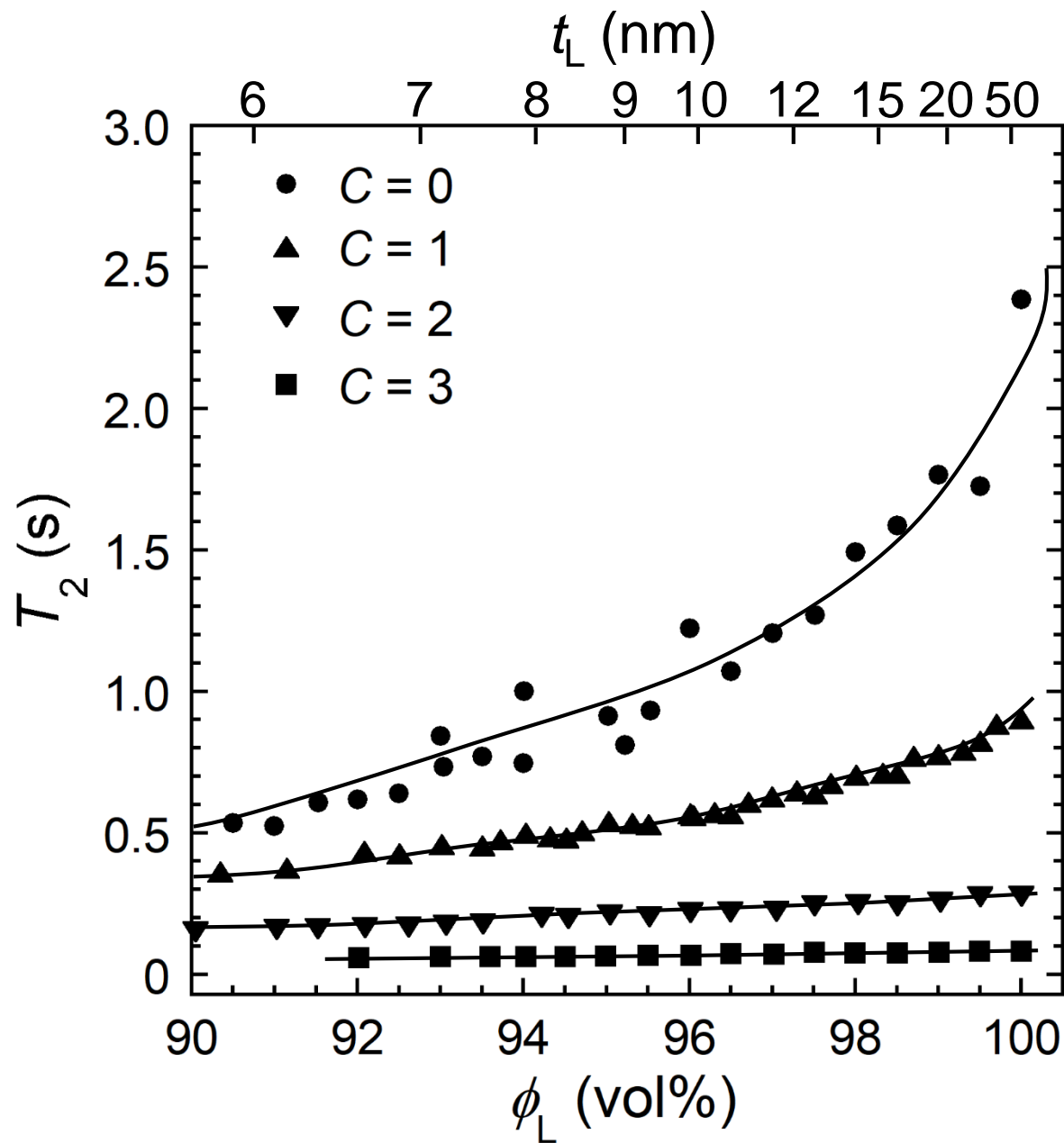


Figure 4(b)

(c) FA + C mol L<sup>-1</sup> LiClO<sub>4</sub> PC solutions

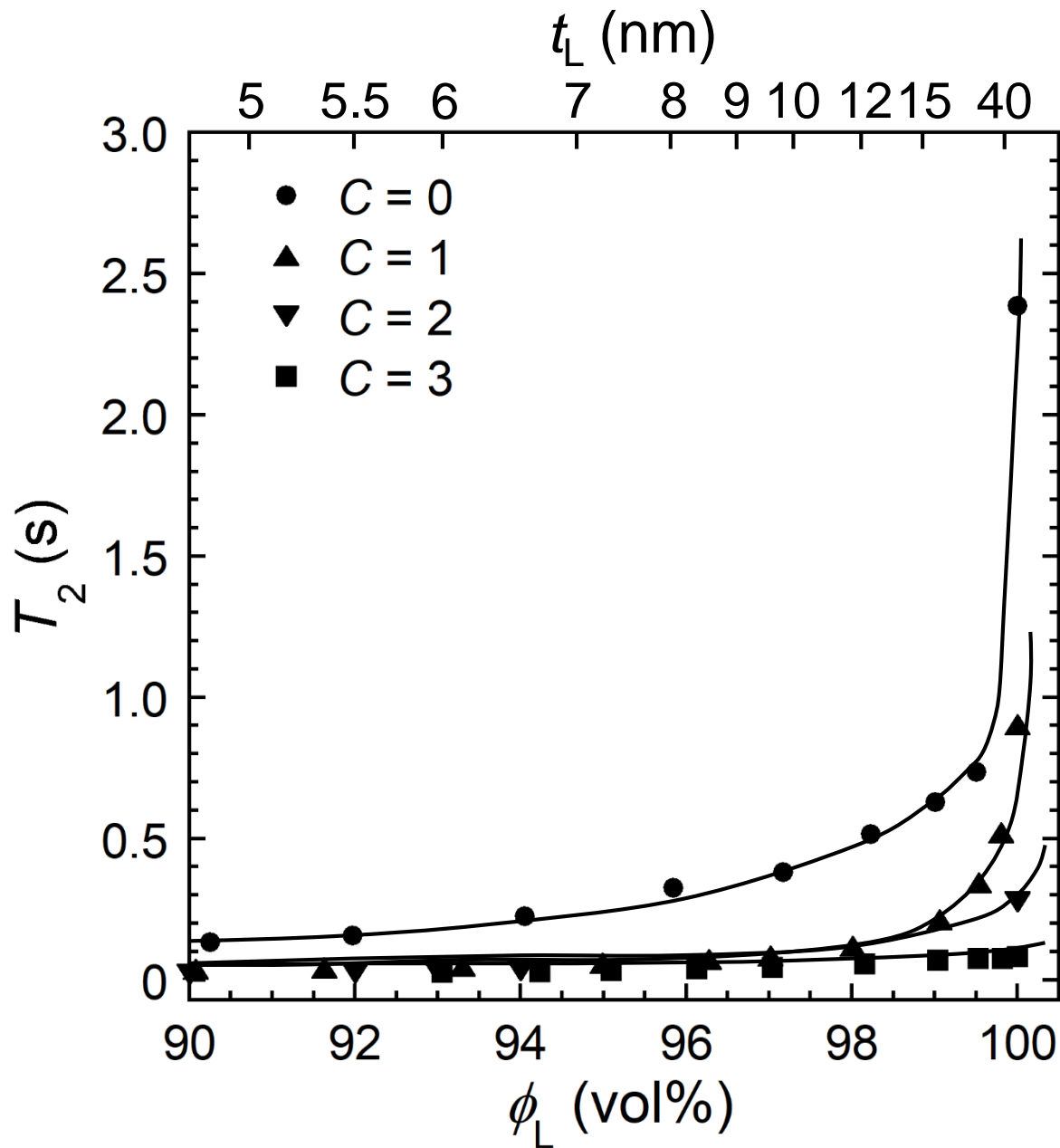


Figure 4(c)

(d) FT + C mol L<sup>-1</sup> LiClO<sub>4</sub> PC solutions

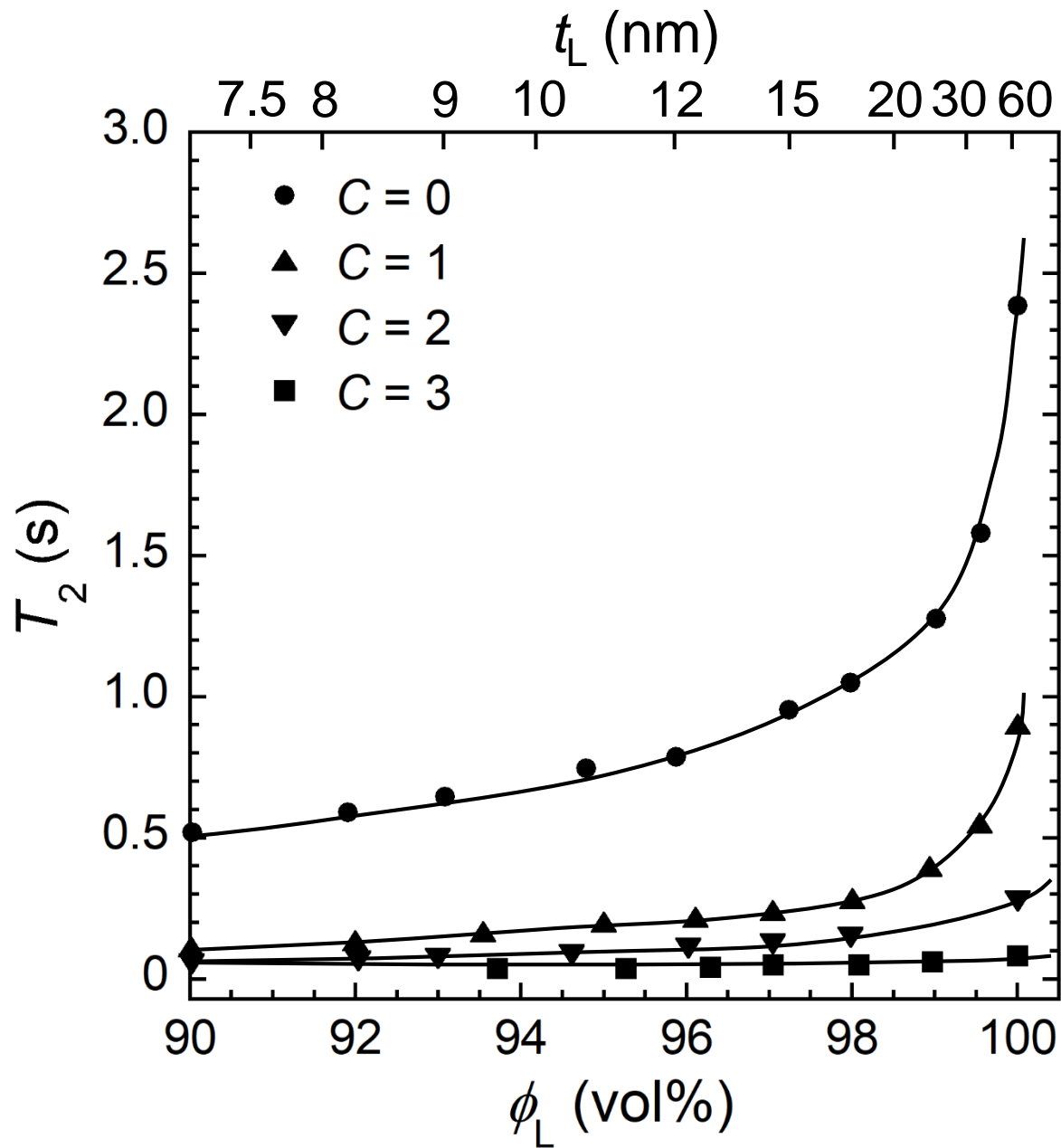


Figure 4(d)

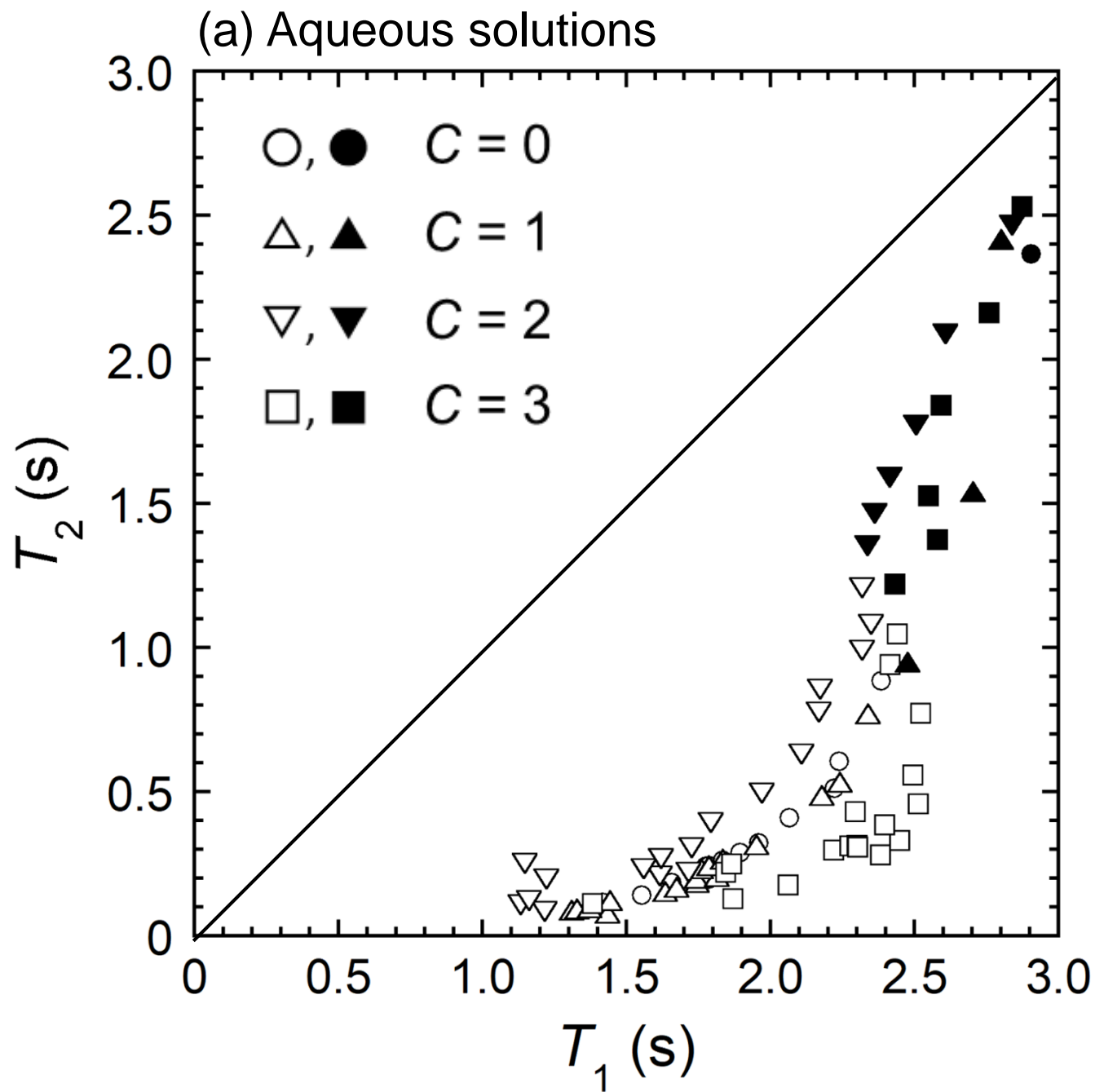


Figure 5(a)

(b) PC solutions

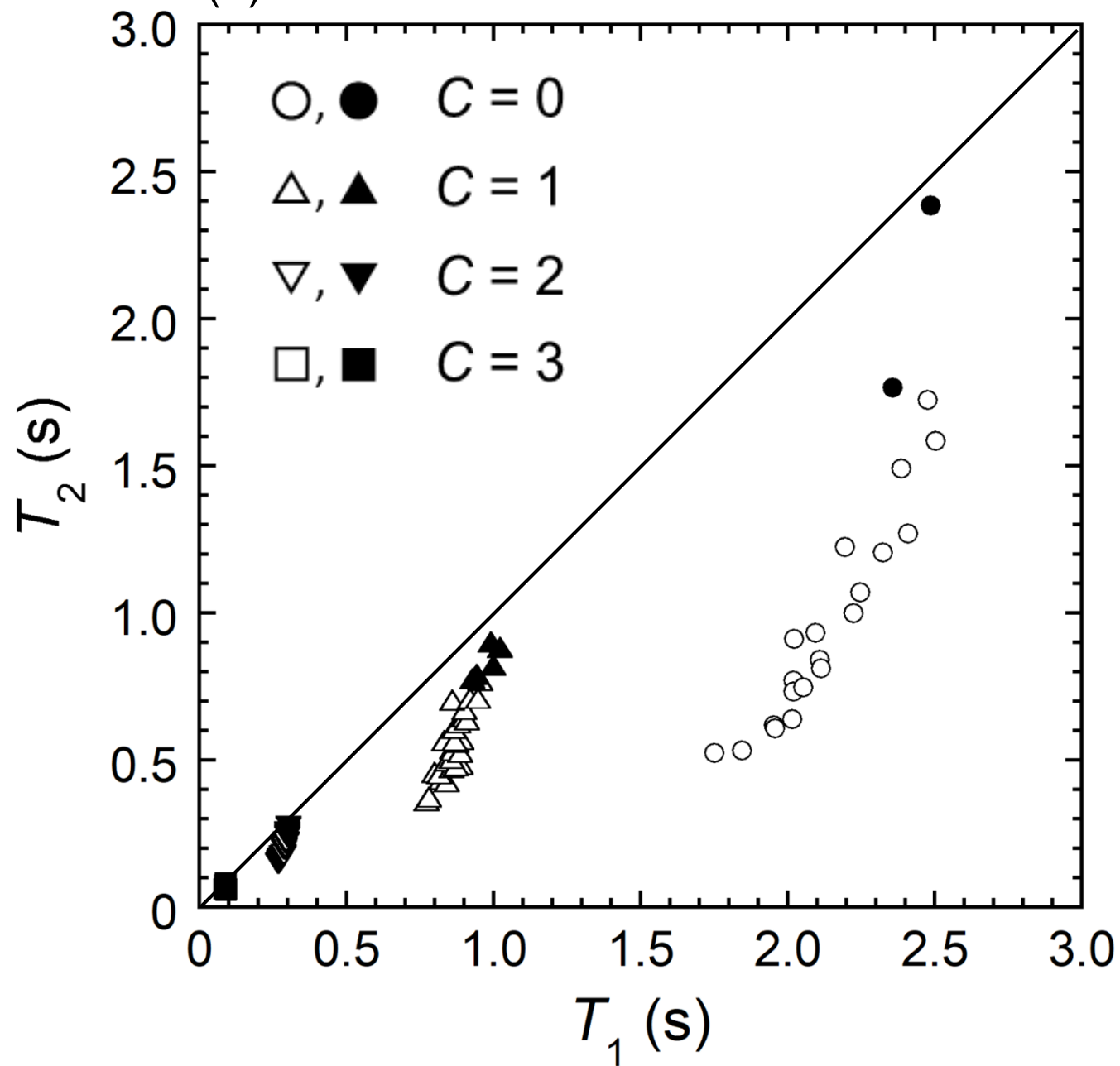


Figure 5(b)

(a) FS + C mol L<sup>-1</sup> LiClO<sub>4</sub> aqueous solutions

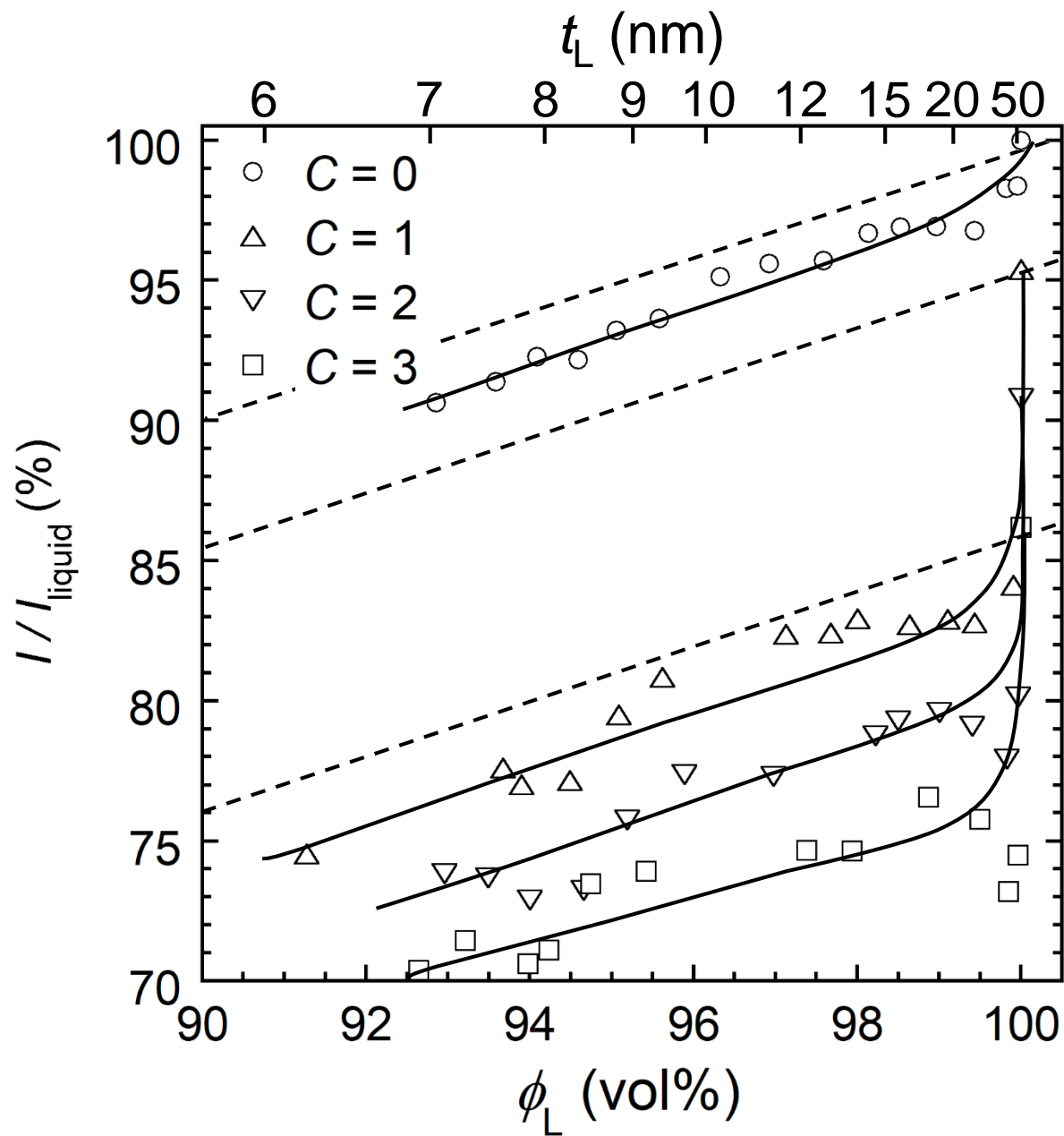


Figure 6(a)

(b) FS + C mol L<sup>-1</sup> LiClO<sub>4</sub> PC solutions

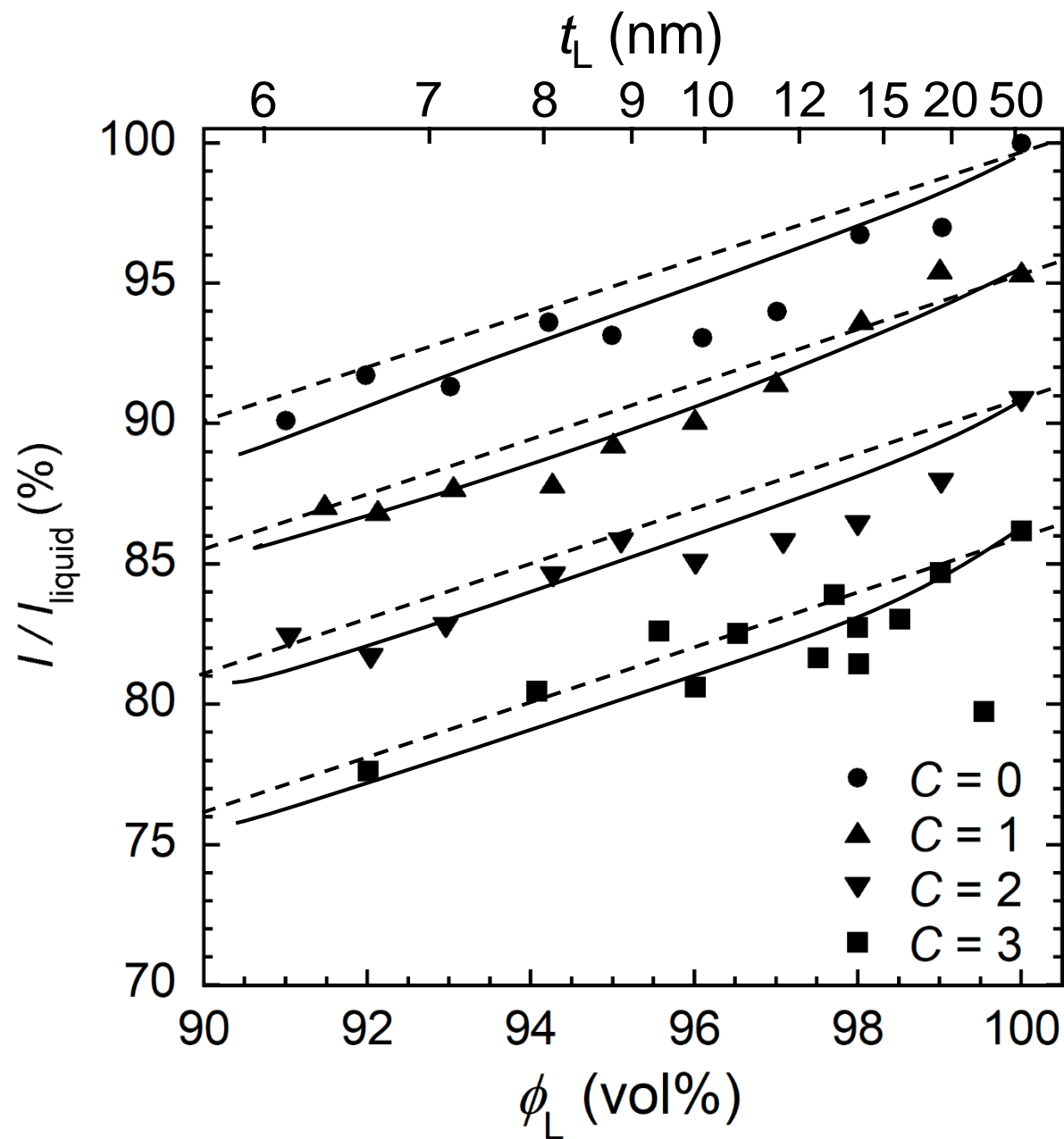


Figure 6(b)

(c) FA + C mol L<sup>-1</sup> LiClO<sub>4</sub> PC solutions

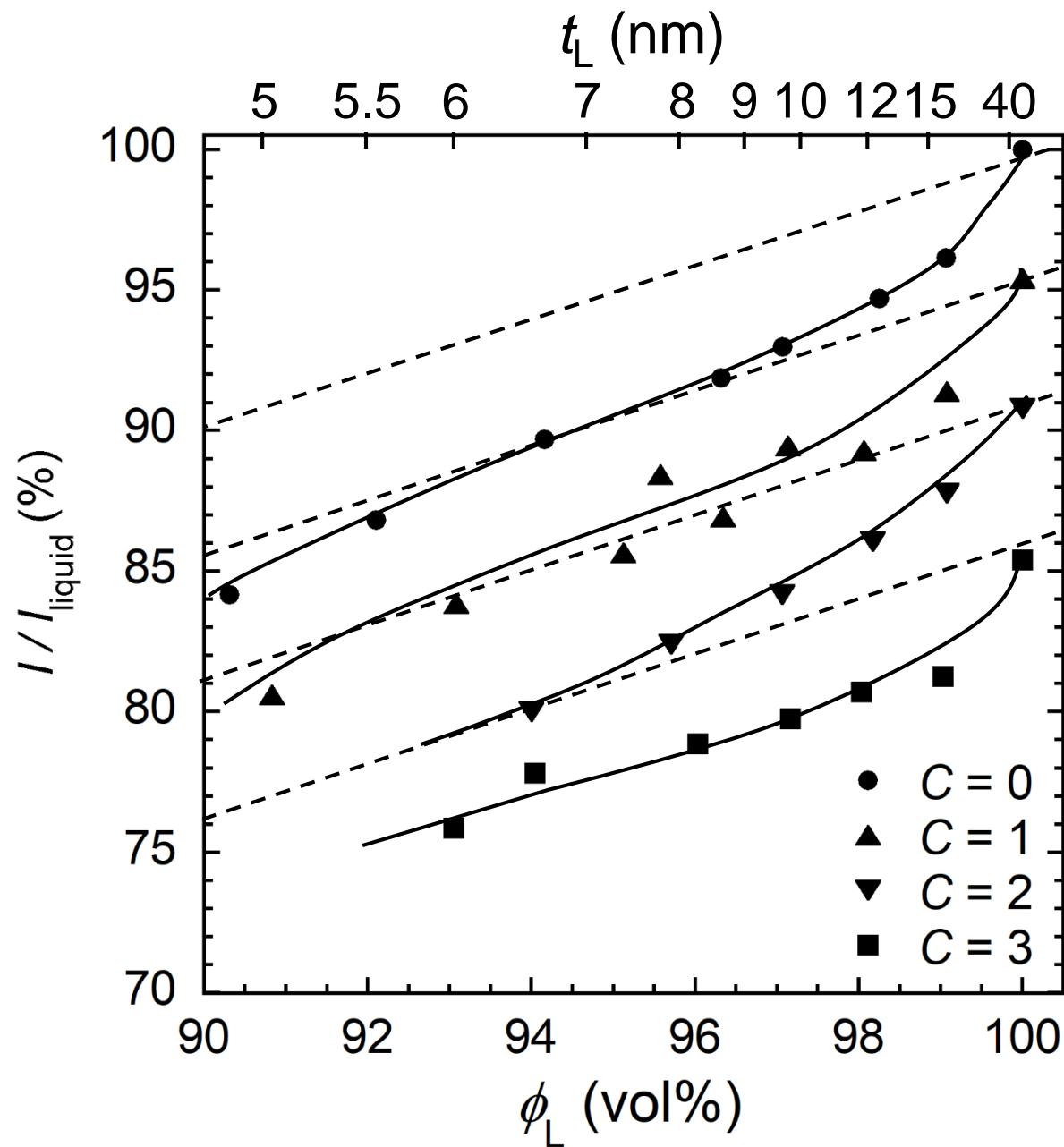


Figure 6(c)



(d) FT + C mol L<sup>-1</sup> LiClO<sub>4</sub> PC solutions

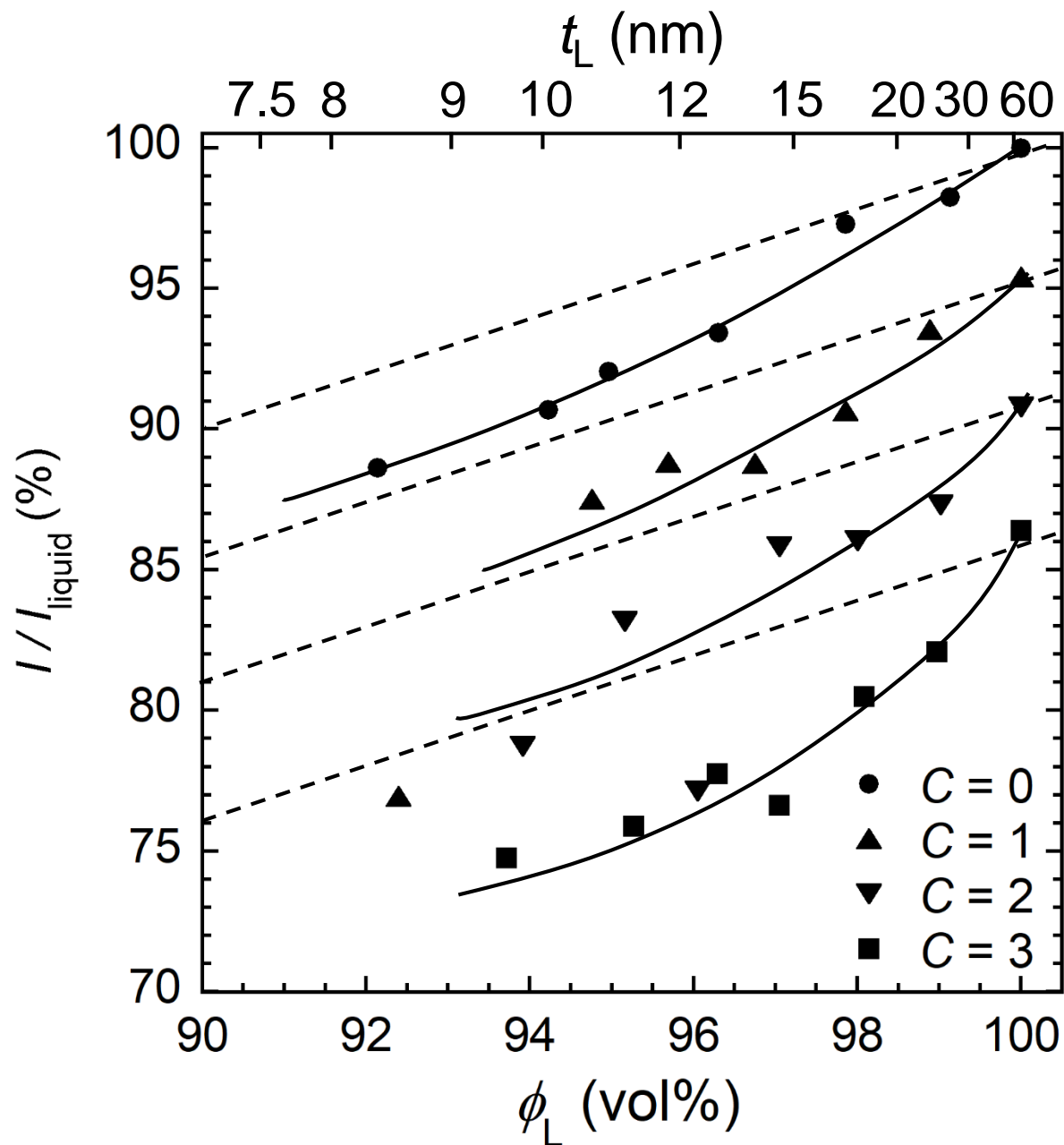


Figure 6(d)

(a) PC in FS

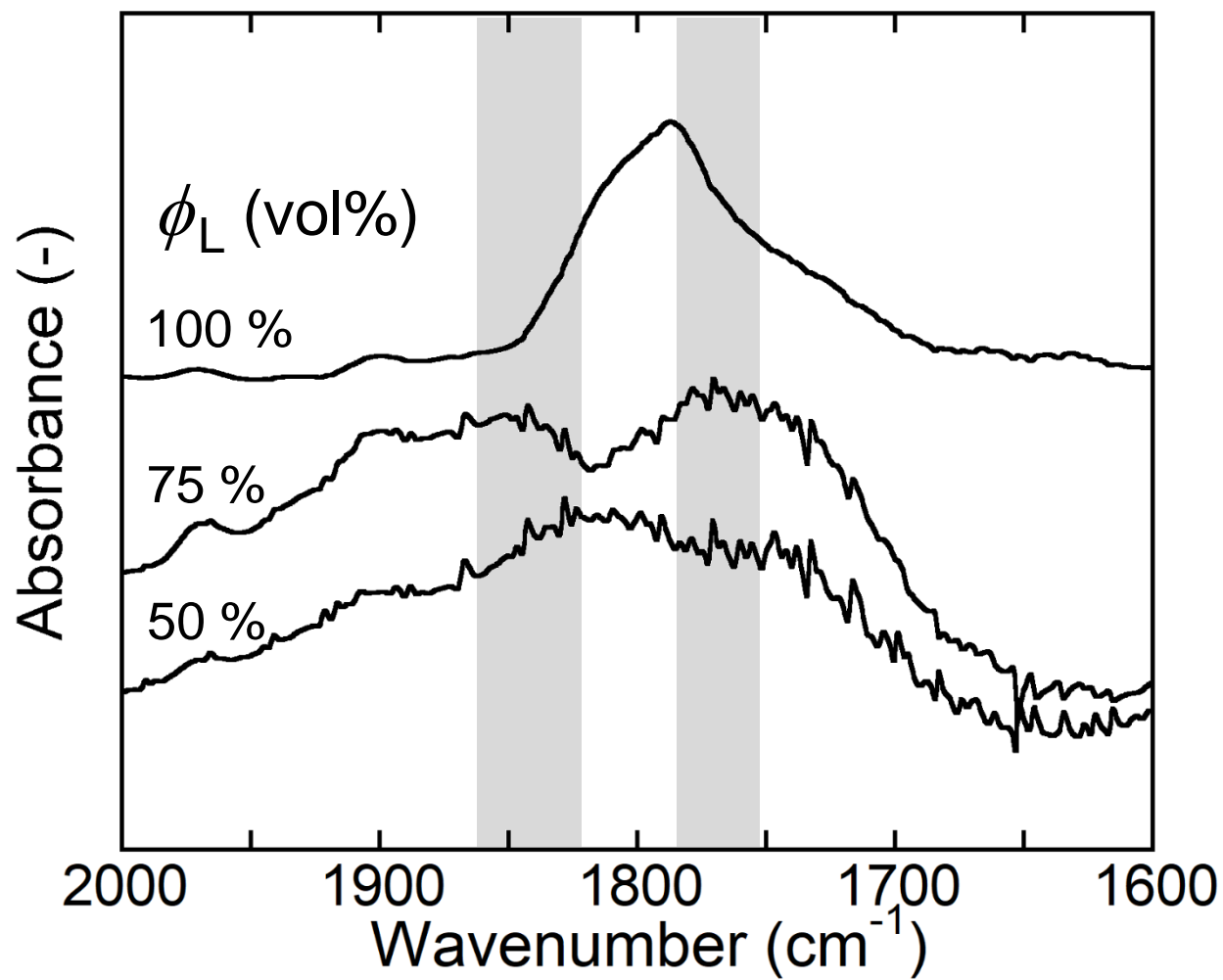


Figure 7(a)

(b) PC in FA

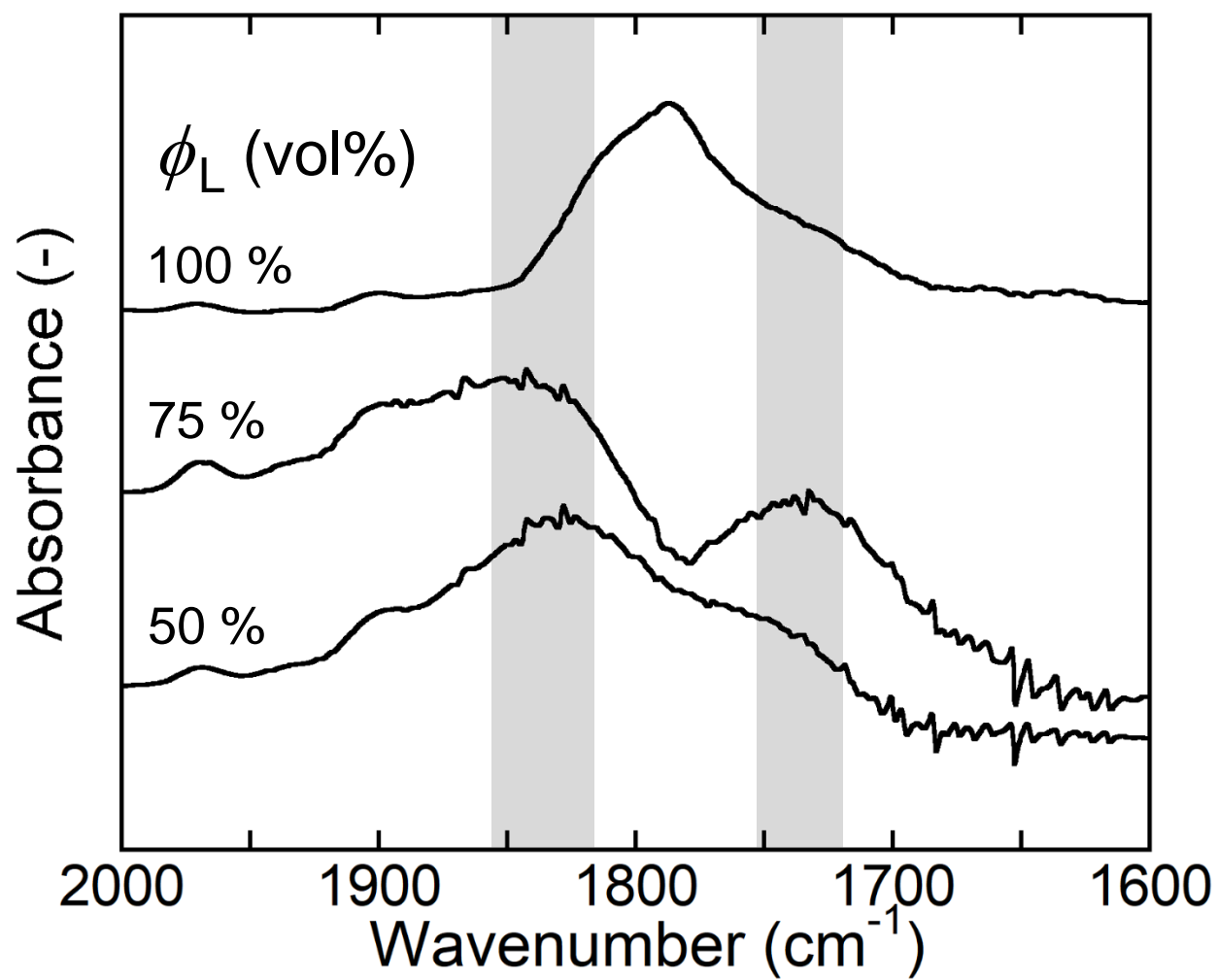


Figure 7(b)

(c) PC in FT

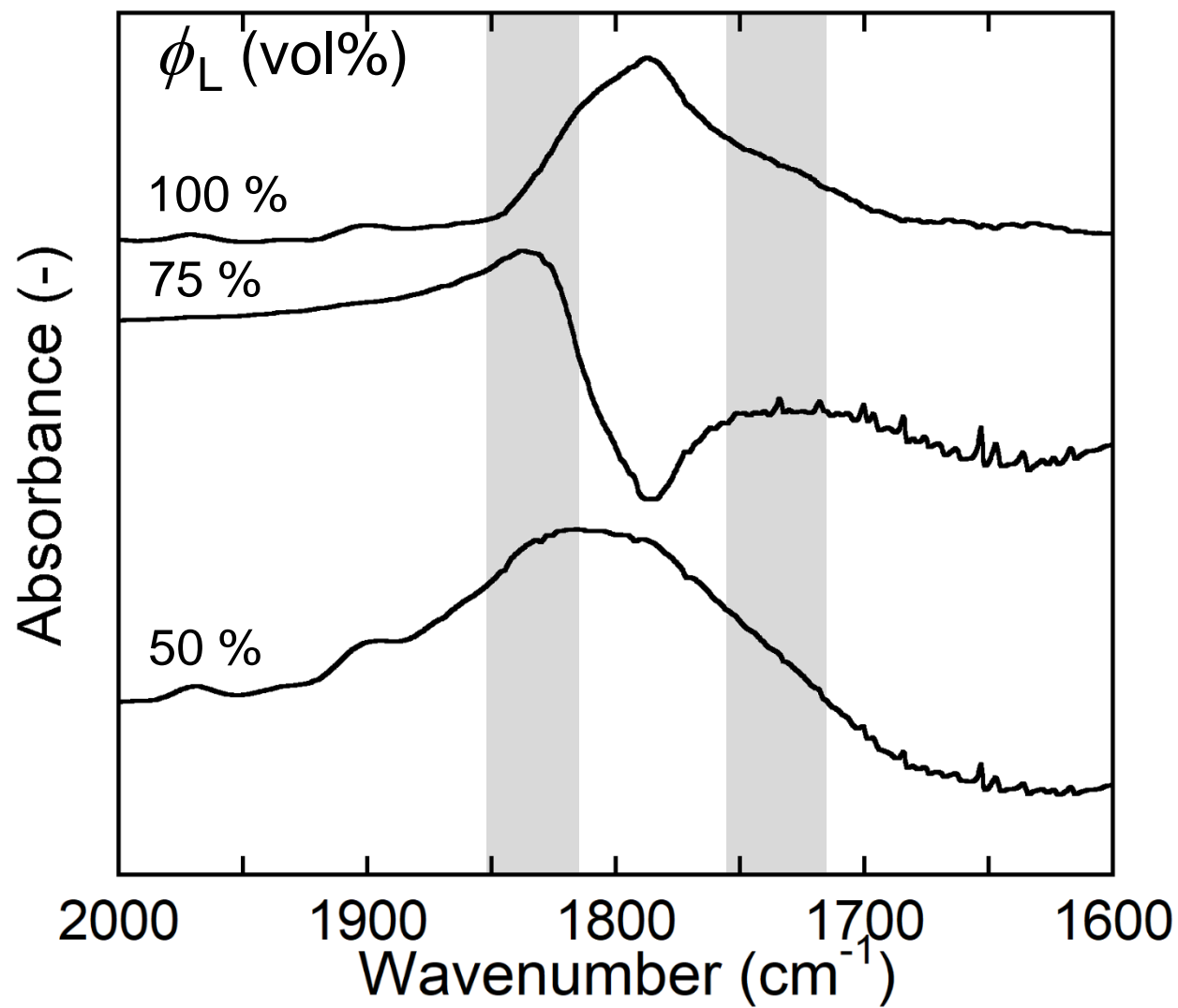


Figure 7(c)

***Colloids and Surfaces A:  
Physicochemical and Engineering Aspects***

***Supplementary Material***

**Solvent molecule mobilities in propylene carbonate-based electrolyte  
solutions coexisting with fumed oxide nanoparticles**

Hideshi Maki<sup>a,b,\*</sup>, Marie Takemoto<sup>b</sup>, and Minoru Mizuhata<sup>b</sup>

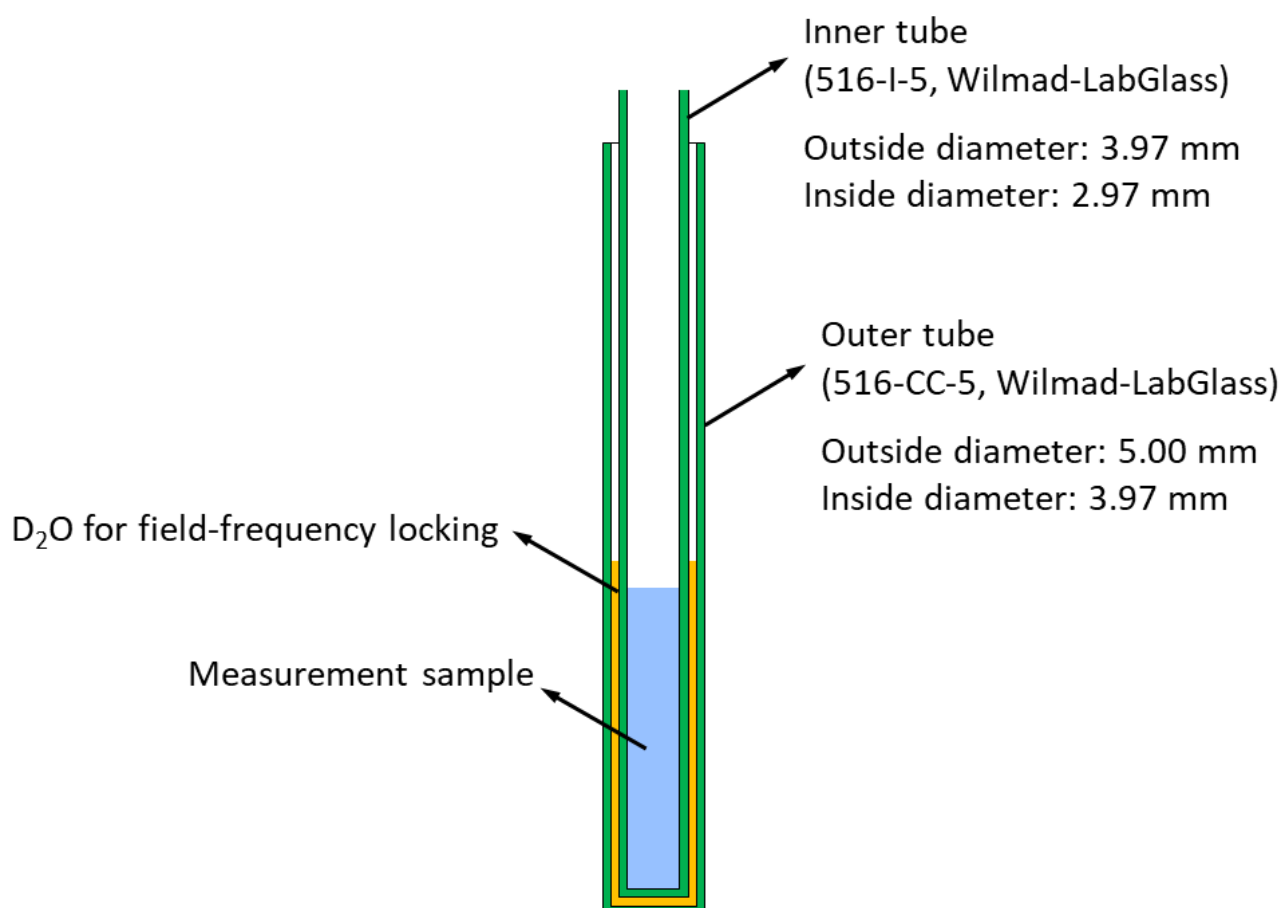
<sup>a</sup>Center for Environmental Management, Kobe University, 1-1 Rokkodai-cho, Nada-ku,  
Kobe 657-8501, Japan

<sup>b</sup>Department of Chemical Science and Engineering, Graduate School of Engineering,  
Kobe University, 1-1 Rokkodai-cho, Nada-ku, Kobe 657-8501, Japan

\*Corresponding author: maki@kobe-u.ac.jp

Table S1. Physical properties of fumed oxides as solid phases which are officially announced value from Evonik Industries AG as manufacturer.

	Fumed silica (FS) AEROSIL® 200CF	Fumed alumina (FA) AEROXIDE® Alu 130	Fumed titania (FT) AEROXIDE® TiO <sub>2</sub> P 90
Average primary particle diameter (nm)	12	10	15
Specific surface area (m <sup>2</sup> g <sup>-1</sup> )	200 ± 25	130 ± 20	90 ± 20
Density (g cm <sup>-3</sup> )	2.2	3.3	4.1



Scheme S1. Coaxial NMR tube system to avoid the contamination of  $D_2O$  for field-frequency locking into the measurement samples.

## ● Hexagonal closest packing model

Apparent average liquid phase thickness :  $t_L$

Average primary particle diameter of solid phase :  $r$

Volume of primary particle as solid phase :  $4/3\pi r^3$

Length of one side of unit cell :  $a = 2\sqrt{2} (r+t_L)$

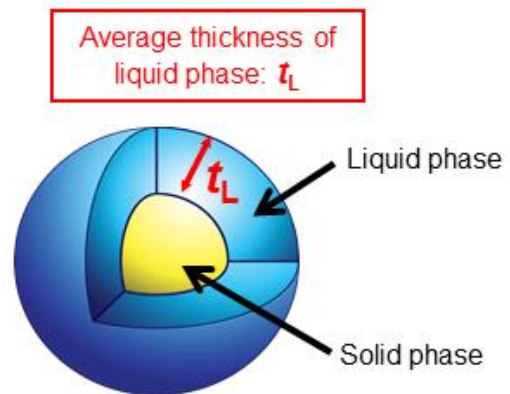
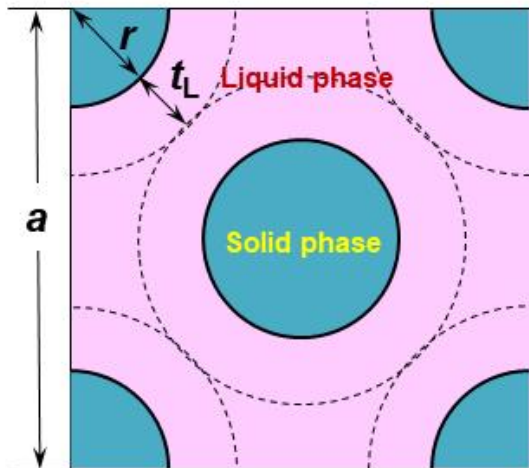
Total volume of unit cell :  $V = a^3 = 16\sqrt{2} (r+t_L)^3$

Volume fraction of solid or liquid phase :  $\phi_S, \phi_L$

Solid particle number per unit cell : 4

$$\phi_S = 1 - \phi_L = \frac{4 \times 4/3\pi r^3}{16\sqrt{2}(r+t_L)^3} = \frac{\pi r^3}{3\sqrt{2}(r+t_L)^3}$$

$$t_L = \left[ \left[ \frac{\pi}{3\sqrt{2}(1-\phi_L)} \right]^{1/3} - 1 \right] \cdot r$$



Scheme S2. Derivation of the apparent average liquid phase thickness,  $t_L$ , by the hexagonal closest packing model.



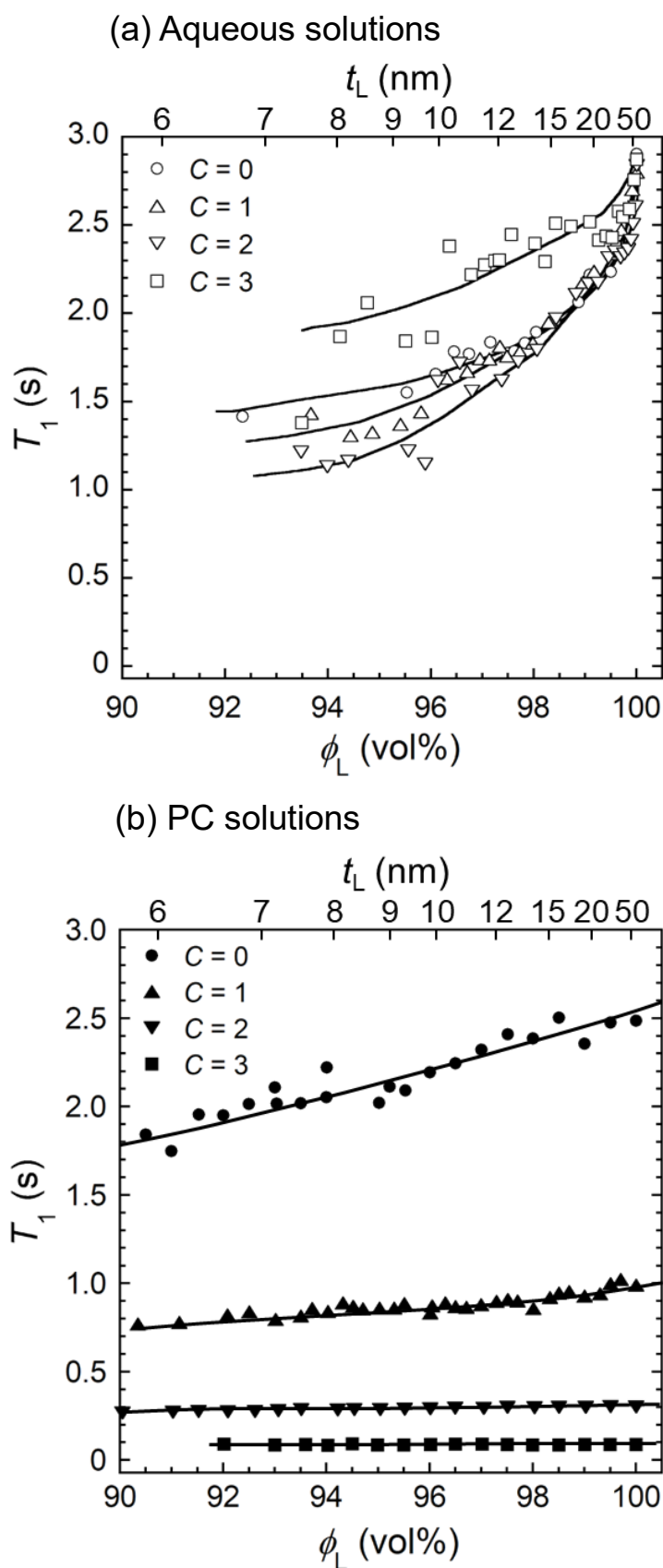


Fig. S1.  $\phi_L$  dependence of the spin-lattice relaxation time,  $T_1$ , of  $^1\text{H}$  NMR due to PC molecule in the FS +  $C$  mol/L  $\text{LiClO}_4$  aqueous or PC solution systems ( $x = 0-3$ ). (a) Aqueous solution, (b) PC solution.